

7

NON-EQUILIBRIUM STRUCTURES*

7.1 Introduction

Studies of molecular structures at or near their equilibrium configurations have long provided information on their geometry in terms of bond distances and angles. Far-from-equilibrium structures are relatively unknown—especially for complex systems—and generally, neither their dynamics nor their average geometries can be extrapolated from equilibrium values. For such non-equilibrium structures, vibrational amplitudes and

* Parts of this chapter have been adapted from Ruan, C.-Y.; Lobastov, V.A.; Srinivasan, R.; Goodson, B.M.; Ihee, H.; Zewail, A.H., *Proc. Natl. Acad. Sci. USA* **2001**, *98*, 7117.

bond distances play a central role in phenomena such as energy redistribution and chemical reactivity. UED provides a direct method for probing the nature of complex molecules far from equilibrium. Before considering specific examples of non-equilibrium structural determination, it would be instructive to discuss some key concepts underlying structures at equilibrium and those far-from-equilibrium.

7.2 Concepts of Equilibrium *vs.* Non-equilibrium Structures

In this discussion, we will classify molecular structures into the following four cases:

- (a) Equilibrium, Boltzmann distribution (Type I)—Cold Ground State;
- (b) Equilibrium, Boltzmann distribution (Type II)—Hot Ground State;
- (c) Non-equilibrium, non-Boltzmann distribution (Type I)—Inverted population, ‘negative temperature’; and
- (d) Non-equilibrium, non-Boltzmann distribution (Type II)—Bifurcation of internuclear distances

Differences between diffraction patterns of structures at equilibrium and those far-from-equilibrium can be understood by first considering the case of a single bond (Figs. 7–1 and 7–2). The diffraction of structures far from equilibrium manifests itself as

- i*) increased damping of the oscillating molecular scattering signal; and

ii) apparent shifts in internuclear distance(s).

As seen in Fig. 7-1, simple thermal heating of the molecule results in nearly the same average internuclear distance, but its vibrational amplitude increases with temperature. This elevated l value can be readily observed as enhanced damping of $sM(s)$; the relevant dependence is given by:

$$sM(s) \propto \exp\left(-\frac{1}{2}l^2 s^2\right) \cdot \frac{\sin(sr)}{r} \quad (7-1)$$

This damping is mirrored as broadened peaks in the $f(r)$ curve because of its Fourier (sine) transform relation to $sM(s)$. The damping reflects thermal averaging over the vibrational states in a Boltzmann distribution, given in the harmonic diatomic limit (l_h) as:¹

$$l_h^2 = \frac{h}{8\pi^2 \mu \nu} \coth\left(\frac{h\nu}{2kT}\right), \quad (7-2)$$

where μ is the reduced mass, ν is the vibrational frequency, k is the Boltzmann constant, and T is the vibrational temperature. In the limit of high energy, l_h scales as the square root of the vibrational temperature. In contrast to this thermal (Boltzmann) limit where the structures are near equilibrium, structures far-from-equilibrium would result if the system were

created with inverted (non-Boltzmann) distributions.

Figures 7–1 and 7–2 show our calculations for the case where wave packets are produced with Gaussian energy distributions at different mean energies, which, in turn, give rise to the corresponding probability densities in the long-time limit. Significantly inverted populations would lead to a clear bifurcation of the internuclear density, inducing splitting and shifting of peaks in the $f(r)$ curve. However, in the case where these non-Boltzmann populations occur at relatively low energies in the potential well, the density bifurcation becomes narrower, and the $f(r)$ curve may not display shifted peaks, but would exhibit increased damping—thus mimicking Boltzmann distributions albeit with exceptionally high l values. These concepts of enhanced damping and shifted bond distances, shown here for a molecule with a single bond far from equilibrium, are directly relevant to complex molecular structures where energy redistribution may or may not be complete, and where certain bonds determine the reaction coordinate.

In what follows, we discuss the UED determination of non-equilibrium structures of types I and II. UED Studies of transient structures for two cyclic hydrocarbons at high internal energies reveal markedly different structural behavior. For cyclohepta-1,3,5-triene (CHT), excitation results in the formation of hot ground-state structures (Scheme 7–1) with bond distances similar to those of the initial structure (non-equilibrium, Type I). In

contrast, cyclohexa-1,3-diene (CHD) undergoes a ring-opening reaction (Scheme 7–2) to form hexa-1,3,5-triene (HT) in its far-from-equilibrium state, as manifested by an inverted population in the torsional degrees of freedom and by highly elevated vibrational amplitudes (non-equilibrium, Type II).

7.3 Experimental Methodology

UED data were obtained with our third-generation apparatus. Samples of CHT (Fluka, 95%) and CHD (Aldrich, 97%) were degassed with several freeze–pump–thaw cycles, and high-purity xenon (Spectra Gases, 99.999%) was used as an atomic reference gas. The nozzle temperature for the diffraction experiments was maintained at 130 °C and 120 °C for CHT and CHD, respectively. To establish the point of reference for temporal studies, the zero-of-time was determined via photoionization-induced lensing of the undiffracted electron beam using CF₃I gas (Aldrich, 99%).

7.4 Data Processing and Analysis

A. Background Subtraction

A significant, slowly-varying background curve underlies the (structurally relevant) molecular interference pattern at each time point. These seemingly time-delay-dependent background curves probably originate from two major potential sources: (1) the shift of the residual background

seen in the ground-state diffraction pattern, possibly caused by the defocused photo-electrons (as well as the stray photo-induced spurious electron emission from the surface of the vacuum chamber); and/or (2) an artifact of the ion-lensing effect. For quick examinations of the data, the slowly varying background curves are removed by fitting the difference data set with 4th-order polynomials. Once the background curves are removed, the remaining high-frequency oscillation patterns for the 75–400 ps data set are almost identical (both in period and in amplitude). This procedure thus highlighted the robustness of the interference terms in the data, independent of the spurious background counts.

B. Generation of “Product-Isolated” Curves from Diffraction Difference Signals

The structure-rendering procedures used for the CHD data have been modified from our previously reported schemes in two aspects. First, the diffraction-difference scheme is extended to include *both* difference curve and “product-isolated” curve procedures. As described previously, the difference curve yields information regarding the proportions of the products obtained following photo-illumination. This procedure may also be used to determine the structure of a given photo-product in a theoretical model, which must include *both* the parent $sM(s)$ curve and that of the product. Both the

experimental difference data [which is produced, for example, by subtracting positive time data (contributed mostly by the parents, with the remaining ~1–15% coming from the photo-products) from the negative time data (100% parent)] and the corresponding curve generated from a theoretical model are comprised of 50% parent contributions and 50% product contributions. The diffraction-difference procedure has the advantages of removing systematic artifacts from the raw experimental data set, and of concentrating on the results of photo-reactions by highlighting only those contributions to the molecular scattering signal originating from internuclear distances that change over the course of the reaction. However, the success of this procedure depends on the success of the ground state structure fitting; moreover, the sensitivity with respect to the product structure is reduced by the contribution from the parent signal.

In light of these difficulties, we implemented a second structural fitting loop that permits the contribution from the product only to be extracted from the total diffraction difference curve. In the first step of this new procedure, the values of the parent/product proportions are obtained at each time point from the usual diffraction difference analysis; these values are then used to fit the temporal behavior of the reaction dynamics. The resulting “exponential” temporal curve is then used to obtain “true” values for the proportions of parent and product species at each point in the reaction. Next

(at each point in the reaction), the parent-only signal obtained at negative time points is scaled down according to the temporal curve and subsequently added to the difference curve at a given time point—effectively canceling out the parent contribution, and leaving only the products to contribute to the diffraction signal. Finally, the product signal is fit (see below). These two fitting loops are connected interactively for successive refining; the refinement is repeated iteratively until the fits converge. The advantages of the new product-isolated procedure are four-fold:

- (1) The experimental data is comprised of 100% products, giving greater sensitivity for studying the product structure(s) directly (particularly when the structural change is significant);
- (2) It provides a more intuitive framework for analysis and interpretation;
- (3) The data analysis is much less dependent on the parent structure fitting; and
- (4) It allows us to exploit the fact that the temporal behavior of the *entire reaction* is known with greater precision than that of the species distribution at any given time point.

C. Novel Aspects of the Product Structure Analysis Used for “Hot” HT Product

The second major deviation in data analysis from our previous methods is the inclusion of non-single-gaussian probability functions for certain bond distances and those for the primary torsional angles. The *former* attempts to take into account the possibility of inverted (non-Boltzmann) vibrational populations in a given portion of the vibrational manifold relevant to our investigation; the *latter* accounts for the distribution of HT conformers. Additionally, an alternative structure modeling/fitting scheme aimed at treating complicated molecular systems is proposed in this work; the methodology and its results should complement the current approach and will be mentioned later.

Before going further, it should be mentioned that these increasingly sophisticated procedures were implemented only after exhaustive attempts to fit the data with our previous, more conventional methods were determined to be unsatisfactory. In our earlier approaches with the CHD data, equations governing geometrically consistent models were carefully constructed for CHD, *cZc*, *cZt*, and *tZt*; these models were then introduced into the UED fitting program in the usual way (these models were independently determined to be quite self-consistent, with the greatest error in mathematical self-consistency of predicted distances to be ~ 0.05 Å for one

long-range non-bonded distance in cZc —nearly all other distances were within 0.005 Å for cZc and cZt , and *all* distances for CHD and tZt were within 0.001 Å. The relatively large error of ~ 0.05 Å was accepted because it was shown to be a result of the simplified geometrically-consistent model for cZc/cZt , and not a human error in algebraic formulation). An equilibrated vibrational temperature for the HT products was estimated to be ~ 2100 K, considering the left-over deposited energy and the vibrational frequencies of the 36 modes. Reasonable values for the mean amplitudes of vibration and the temperature corrections to the distances were obtained by meticulously constructing U-matrices for entry into ASYM40, along with appropriate Hessians from Gaussian for each species. Structural parameters for the various species were obtained from conventional electron diffraction, our own fit of the ground state, and from *ab initio* calculations. We could then perform our early fits, in which we could see qualitatively: (1) that the progress of the reaction was relatively slow (indeed, the time constant for the reaction was always in the ballpark of 30 ps, regardless of the model); (2) that the positive and negative contributions to $\Delta f(r)$ were consistent with ring-opening; and (3) that fitting the $\Delta f(r)$ curves to the different conformers gave relatively poor agreement (considering our signal-to-noise ratio) to the various possible static structures, but seemed to support cZc more than anything else.

The double-Gaussian probability distribution function for bond distances

In this approach, for each of the direct-bond distances in the CC skeleton, a double-Gaussian probability function is assigned; this may be compared with the single-Gaussian probability functions (characteristic normal Boltzmann thermal populations) normally used in static electron diffraction. The double Gaussians were allowed to vary in their mean positions and FWHMs, thereby giving the refinement freedom to qualitatively simulate an inverted vibrational population in which the density bifurcates towards the classical turning points of the local potential well. Naturally, if the mean positions of the two Gaussians merge together, then the normal single-Gaussian picture for a Boltzmann vibrational distribution is recovered.

The conformational evolution—analysis of the torsional angle distribution

The *first* novel analysis of the structure and torsional angle distribution (which ultimately reflects the HT conformer distribution) was performed as follows. The geometrically-consistent model of the generalized HT (specifically, *cZt*) structure was put into the refinement routine. For each of the two torsional motions under consideration [i.e., those involving rotation about the two C–C single bonds, namely through the torsion angles $\tau_1(\angle C1=C2-C3=C4)$ and $\tau_2(\angle C3=C4-C5=C6)$], a two-peak cyclic Gaussian

probability function was assigned, with mean positions centered (and fixed) at 48° (*cis*-) and 180° (*trans*-). Additionally, the distributions of these angles were fixed at 40° (FWHM); giving a distribution shown to give a better fit than that obtained by assuming delta functions for the dihedral angle distributions (but the value of 40° was not numerically optimized). The mean angle values, determined from *ab initio* calculations, and FWHM values, were held fixed at this stage in the processing in order to reduce the number of adjustable parameters. The weighing prefactors before the *cis*- and *trans*-normalized Gaussian functions were allowed to vary (but naturally were required to have a sum of 1). The two torsional motions were regarded as independent. With $2 \times 2 = 4$ weighing prefactors (only two of which are independent parameters), the relative portions of the *cZc*, *cZt*, and *tZt* conformers could then (in principle) be determined.

With the increased complexity of the total fit, each major step within the complete iterative refinement is broken into smaller steps according to the sensitivity of the fit to each given type of parameter; i.e., in terms of the fit sensitivity, product fraction > bond distances > torsional angles / conformational prefactors (standard three-atom bond angles, which do not differ more than a few degrees among the different HT conformers, were held fixed at the *ab initio* values). The low-frequency (DC) background-removing procedures (and convergence tests for avoiding divergence) are embedded

within the fitting iteration cycles for guidance towards the global minimum. For the sake of objectivity, the exact refinement sequences are directly coded into the software so that all time points are treated equivalently.

At this stage of structural refinement, there were 18 total independent fitting parameters. These included: 3 independent covalent C–C bond distributions (C1=C2, C2–C3, and C3=C4), each described by 2 independent Gaussians [with their own mean values (2 parameters), FWHMs (2 parameters), and relative amplitudes (1 parameter)], giving 15 independent parameters for the covalent distances; torsional prefactors for the conformational distribution (described by 2 independent parameters); and finally the fraction of the product (only 1 parameter for difference curve fitting) ($15+2+1=18$). Other structure parameters were taken from *ab initio* calculations, with the mean amplitudes of vibration estimated using the *ab initio* force constants extrapolated to 2100 K with ASYM40. Although the total number of fitting parameters is large, it was found that only the fraction of the product, the C–C distances, and the torsional prefactors are very important for determining the global outcome of the fit [the other parameters (e.g., the FWHMs and deviations from 50/50 proportionality of the two-Gaussian distributions) can be regarded as mere “by-standers” to the overall fit; however, of course the values of these “secondary” parameters would not be trustworthy if the global structure fitting did not yield good results].

During the structure/conformation refinement of the CHD data, it was found that iterative background-removing procedures and convergence-checking procedures were crucial for the ultimate success of this step-wise process.

D. The Generalized Monte Carlo Method: A Complementary Analysis

Although the significant features observed from the aforementioned modeling scheme should be robust, one could argue that certain *specific* structure features might originate from the specific assumptions and constraints we have applied in the model (e.g., the values and distribution of the torsional angles and the bifurcation of the C–C bond distance probability function). Thus, it could be argued that there might be yet *other* (improved, or at least equally good) minima in the χ^2 hypersurface in the configuration space that are also well justified by the quality of our experimental data—and would be located if the structure were described differently—but are not reachable under the current constraints of the model.

In order to alleviate this doubt, global scanning was performed using a Monte Carlo approach over the configuration space (defined by a geometrically consistent *Z*-matrix representation of the structure) to probe for the existence of local minima for in each time delay. The *Z*-matrix representation of molecular structures is widely used in many *ab initio* and semi-classical methods in optimizing molecular geometry and dynamics. The

flexibility of this construction allows us to treat least-squares refinements of UED in the molecular hyper-configurational space, and to survey the landscape of the χ^2 hypersurface. By examining all the possible minima, the *model-dependent* “correlations” among structure parameters (e.g., pairs of similar covalent bond distances) can be noted for further analysis; moreover, the universal structure features, which should be *model-independent*, can also be established; the Monte Carlo survey helps us to locate the true, global minimum and allows us to report global structure features with a high level of confidence.

This new modeling procedure has been applied to analyze our CHD data with two different initial conditions for the HT structure: 1) the *ab initio* structure of *tZt*; and 2) the *ab initio* structure for *cZc* (both refinements gave similar results). Unlike conventionally applied least-squares fitting routines, no non-thermal probability distribution functions are presumed in the initial models. Additionally, this approach has the “built-in” predisposition of treating all dynamical effects as being effectively averaged, providing a single, static framework for the molecule (e.g., there are no distributions assigned to the dihedral angles—instead, average values are directly determined for τ_1 and τ_2 for each minimum on the χ^2 hypersurface).

Even without the assumption of non-thermal probability distribution functions, the averaged structure revealed in this complementary analysis

shows clearly that one C–C single bond is extended to 1.7–1.8 Å, with the other C–C single bond varying between 1.35–1.45 Å; additionally, the average skeletal structure of the HT product clearly takes on the shape of some intermediate structure between that of the “static” *cZc* and *cZt* conformers. These results are robust and apply for nearly all the time frames. Those averaged (static) general characteristics are very consistent with the results obtained with the dynamically resolved non-thermal model.

7.5 Results and Discussion

A. Ground States of CHT and CHD

Figures 7–3 and 7–4 show typical ground-state diffraction images for CHT and CHD and the corresponding structures. Differences between the ring patterns of the two species are evident even in the 2D images, demonstrating the high sensitivity and resolution of our third-generation UED apparatus. Moreover, these three systems have no heavy atoms, and the diffraction, which is from only C- and H-atoms, is sensitive to the increased complexity of these two structures.

The major peaks in the $f(r)$ curves reflect relative populations of various C–C distances in these complex molecules. In CHT, for example, covalent C–C distances occur at ~ 1.4 Å, second-nearest neighbor at ~ 2.5 Å, and third-nearest neighbor at ~ 3.0 Å. The $f(r)$ curve for CHD (with one less C-

atom in the ring) clearly shows much lower density of third-nearest neighbor C···C distances compared to CHT, in good agreement with results obtained with conventional electron diffraction^{2, 3} and our own *ab initio* calculations. Figures 7–5 and 7–6 show the refined ground-state structures of CHT and CHD, along with the best-fit bond distances and angles, together with theoretical predictions.

B. Structural Dynamics of CHT

Upon excitation, CHT undergoes an ultrafast hydrogen shift,^{4,7} but with subsequent reformation of CHT at high internal energy. Except for their relative intensities, all the product-only $sM(t; s)$ curves were nearly indistinguishable. Figure 7–7 shows the experimental $sM(s)$ curve averaged from 75 to 400 ps, along with theoretical curves with the same internuclear distances as those of the initial structure,² but with varying l values. It is evident that the experimental curve is significantly more damped than the theoretical curve (for the initial structure) at 403 K, clearly establishing the “hotness” of product CHT. If the initially deposited energy (107 kcal/mol) were equipartitioned among the CHT modes⁸ with a Boltzmann distribution within their vibrational levels (*c.f.* Fig. 7–1), the molecule would have an internal temperature of ~2200 K (per mode). However, the poor fit of this thermalized model with our experimental data precludes Boltzmann

vibrational distributions.

Indeed, excellent agreement is obtained between experiment and theory with l values whose mean is nearly three times that at equilibrium, indicating a non-Boltzmann distribution in the vibrational levels (see Fig. 7–8). This dramatic increase in the vibrational amplitudes compared to those resulting from a Boltzmann assumption suggests that the hot (product) structure can be characterized by a negative temperature, wherein the upper vibrational levels have higher population than the lower levels. Note the similarity in frequency components between the theoretical $sM(s)$ curve for the equilibrium structure (at 403 K) and the experimental curve, indicating that internuclear distances (in the product) are nearly identical to those at equilibrium—in turn implying nearly complete energy redistribution.

Figure 7–9 shows the structural evolution of the CHT product, obtained by fitting the growing intensity of the $sM(t; s)$ curves with increasing time delay. Previous ultrafast spectroscopic studies⁵ have suggested that conical intersections are responsible for the ultrafast formation of product in tens to hundreds of femtoseconds. However, our structural dynamics studies indicate that the hot structure must be formed on a time scale of 16 ± 3 ps. This longer time scale implies that the product is formed via an avoided crossing or by longer-lived trajectories on the excited surface that involve intramolecular vibrational energy redistribution (IVR);

see below. This is not surprising as other studies on the femtosecond time scale⁹⁻¹¹ have shown the existence of a distribution of femtosecond and picosecond trajectories as molecules traverse a complex energy landscape. If all trajectories were on the femtosecond time scale and we were merely observing picosecond energy redistribution, our $sM(s)$ curves would have revealed structural changes as a function of time. On the other hand, if the structure were that of the excited state, the vibrational temperature would be much lower than that indicated above. It should be noted that UED probes the changes of *all* nuclear coordinates and therefore, the dynamics reported here are directly relevant to global structural changes in the molecule. In contrast, spectroscopic studies reported for the gas phase⁵ (femtoseconds) and condensed phase⁴ (26 ± 10 ps) monitor state populations. The roles of the solvent and intramolecular relaxation must be disentangled before direct comparisons can be made with our results of the isolated reaction dynamics.

C. Structural Dynamics of CHD

From a purely chemical standpoint, the photo-reaction of CHD is a prototypical reaction for the large field of polyene photochemistry, involving various types of chemicals (including dyes). Generally speaking, this reaction belongs to the family of *pericyclic rearrangements* (reactions believed to proceed with a transition state possessing a closed loop of interacting

orbitals); specifically, the photoreaction of CHD to form HT is known as *electrocyclic ring opening*. In general, the outcomes of pericyclic rearrangements can be predicted by the Woodward–Hoffmann rules, which were constructed using relatively simple molecular orbital symmetry arguments. For example, these rules predict that for a system with $4n$ π electrons (i.e., with two conjugated double bonds in the ring), photochemical ring opening will proceed with *conrotatory* specificity (that is, the ring opening will proceed such that the end groups at the ring opening position will *rotate* in the *same* direction), while systems with $4n+2$ π electrons will proceed via *disrotatory* motion of the end groups (for $n=0,1,2\dots$). The CHD reaction has also been used as a model system for studying the effects of substituents and solvent on the photo-reaction rate. For example, the effects of the presence of solvent on energy redistribution and transport—as well as the effects of friction of the solvent on bulk motion and morphological change of the solute over the course of a chemical reaction—have been studied. Additionally (and of direct relevance to this work), the ultrafast dynamics of this reaction have been studied experimentally and theoretically by a number of groups over the past 10 years, and there appears to be considerable disagreement regarding the interpretation of the various results regarding, for example, the rate of ring opening in the reaction.

The CHD/HT reaction has biological significance as well. Because this reaction is a model for polyene photochemistry in general, it is also relevant to a variety of polyene photo-isomerization reactions critical to various biological processes. Examples frequently cited in the literature include: the photo-isomerization of 11-*cis* retinal (a vitamin A derivative) to form all-*trans* retinal in rhodopsin (the fundamental process in dim-light vision of vertebrates); the photo-isomerization of all-*trans* retinal to form 13-*cis* retinal in bacteriorhodopsin (a fundamental process of photosynthesis in certain types of bacteria); and the *cis-trans* isomerization of urocanic acid in the epidermis by UVB light (a process that has been implicated in the suppression of immune response that ultimately leads to skin cancer). Moreover, the light-induced ring opening of CHD is directly relevant to the synthesis of vitamin D *in vivo*. Specifically, CHD models the chromophoric subunit of 7-dehydrocholesterol, which forms *cZc*-previtamin D upon UV irradiation in the primary step of vitamin D synthesis.

Although photochemical characteristics of CHD were studied long ago, various important investigations regarding its ultrafast dynamics have been carried out within the last decade. The initial UV excitation of CHD in its 1A_1 ground state creates a population in the 1B_2 state, which subsequently “decays” either by rapid motion out of the Frank–Condon region of the excited state potential energy surface, or by ultrafast internal conversion to an

optically forbidden 2A_1 state on a time scale of ~ 10 fs. Many spectroscopic tools encompassing resonance Raman scattering, UV absorption, resonance enhanced multiphoton ionization (REMPI), and dissociative intense field ionization have been incorporated to elucidate the photodynamics of the ring-opening reaction of CHD. The analysis of this reaction is, however, greatly complicated by the effects of vibrational excitation and the lack of information about the spectra of the possible conformers of HT, namely cZc and cZt (the spectrum for the lowest-energy conformer, tZt , is well-known).

One can easily see that *at least* four time scales are involved in this reaction:

- (1) the depopulation of the initially populated 1B_2 state into another excited state (most probably 2A_1);
- (2) the depopulation of the excited state into the vibrationally hot CHD ground state;
- (3) the depopulation of the excited state into the photoproduct of the ring-opening reaction (i.e., the step governed by the all-important ring opening rate); and
- (4) the isomerization of the initially formed photoproduct (most probably cZc) into other isomers (cZt and tZt).

In the condensed phase, the problem is complicated further due to possible

vibrational relaxation (thermalization) caused by the solvent molecules. The apparent difficulties associated with these complicated processes are evident in the fact that the suggested time scales for the processes scatter over an order of magnitude, depending on the detection methods and the various interpretations.

In reactive systems, where bonds are broken and formed, the partitioning of energy may result in its localization in certain bonds associated with the reaction coordinate. Indeed, we observed incomplete energy partitioning even up to 400 ps in hot 1,3,5-hexatriene (HT), formed by the ultrafast ring opening of CHD.¹²⁻¹⁵ Figure 7-10 shows the 2D diffraction-difference images and Fig. 7-11 shows the evolution of radial distribution curves for the ring-opening reaction of CHD. The product-only HT diffraction curves were significantly damped at all time points (manifested as peak broadening in the $f(t; r)$ curves), indicating the vibrationally hot nature of the product structure; however, unlike CHT, new peaks appear in $f(r)$. Shown below the experimental data in Fig. 7-11 are theoretical $f(r)$ curves for three hot conformers of HT (labeled cZc , cZt , and tZt with respect to the conformation of torsion angles about the C-C single bonds; see Fig. 7-15). Close inspection of the experimental $f(t; r)$ curves reveals greater similarity to the theoretical cZc curve than to that of the lower-energy tZt conformer. Furthermore, an anomalous peak at $\sim 1.7 \text{ \AA}$ can be seen as a shoulder in all

the experimental $f(t; r)$ curves; the presence of this peak—which is about 0.2 Å away from expected equilibrium C–C distances—was found to be reproducible in repeated diffraction experiments.

Least-squares refinement of the structural parameters yielded a HT molecular structure at each time slice; to locate the global minimum, Monte Carlo techniques were first applied for searching the configuration space, and finally the structure at each time represents the average over the local minima closest to the global minimum. These HT structures showed no tZt character, but consistently manifested a configuration intermediate between cZc and cZt —far removed from a thermally equilibrated conformer distribution of ~41% tZt , ~45% cZt , and ~14% cZc at 2100 K (estimated from *ab initio* calculations of the conformer energies). Moreover, the ~1.7 Å peak observed in the $f(t; r)$ curves was assigned to one C–C single bond in HT—a highly non-equilibrium value for a C–C internuclear separation. The remarkable departure from the predicted equilibrium conformation, together with the unusual C–C bond length, confirms the far-from-equilibrium nature of the HT structure.

The hot HT structure is formed with a time constant of 32 ± 2 ps (Fig. 7–12) and remains virtually unchanged over the course of the experiment (400 ps) as shown in Fig. 7–13. The refined ring-opened structure of HT is shown in Fig. 7–14, while time-averaged values for selected structural

parameters are summarized in Table 7–1, along with corresponding *ab initio* values for the three HT conformers. The persistence of this far-from-equilibrium structure even up to 400 ps indicates that unlike CHT, energy partitioning within HT is slow with respect to both the rate of product formation and the time scale of the UED experiment. The existence of a *cZc*-like conformation clearly indicates an inverted population on the potential energy surface (projected along the coordinate of torsional motion), with significant density at the classical turning points—this coherent nuclear motion is shown schematically in Fig. 7–15. Moreover, the ~ 1.7 Å distance assigned to a C–C bond would require ~ 15 kcal/mol of the available ~ 90 kcal/mol to be deposited in that C–C bond (assuming a simple Morse oscillator model)—providing further evidence for an inequitable partitioning of energy. Note that if energy partitioning were indeed complete, then each of the 36 modes in HT would have ~ 2.5 kcal/mol.

Coexistence of the two structural features—an inverted torsional conformation and a stretched C–C bond—over time strongly suggests a long-lived, low-frequency hybrid motion comprised of both torsion and asymmetric stretching of the carbon skeleton. Conceptually, one may picture that as the molecule oscillates between the turning points of the potential well (Fig. 7–15), the stretched C–C distance is shifted continuously from one C–C single bond to another and at the turning points, the torsional energy is partially

stored in the C–C bond stretch. That this far-from-equilibrium structure lasts for over 400 ps suggests a bottleneck in energy transfer from the inferred hybrid motion to other (higher frequency) modes, after the initial energy deposition. This energy localization could result from a mismatch in the frequencies of the coherent modes compared to all other modes (at these high internal energies). It is interesting to note here that torsional modes of this type have been isolated in dynamical calculations of polypeptides.¹⁶

Ultrafast spectroscopic studies of the CHD ring opening reaction have suggested contrasting time scales for the formation of the HT product—tens to hundreds of femtoseconds¹³⁻¹⁵ and 6 ± 1 ps¹²—with the presence of conical intersections invoked to rationalize the ultrafast time scales. The initial preparation of CHD is to the S_2 excited state; the S_2/S_1 conical intersection is along the readily accessible symmetric path (see below) and gives rise to femtosecond dynamics. Accordingly, the crossing/avoided crossing to the ground state (S_0) determines the longer (picosecond) time-scale of the dynamics. It is interesting to note that while we found virtually no contribution from hot CHD in the HT product diffraction patterns (despite our sensitivity to hot “parent” structures in CHT), static condensed-phase experiments have reported a 60/40 branching ratio for the CHD reformation/ring-opening pathways.¹⁷ This near-absence of hot parent structures, along with the long time observed by UED for ring opening,

signifies the crucial role played by the solvent (in contrast to the isolated molecule) in redirecting the fate of the reaction. For instance, the increased steric hindrance to ring opening in the solvent may favor the reformation of CHD over ring opening. Moreover, the solvent can induce slight perturbations in the relative positions of the potential energy surfaces, which can dramatically alter the time scales¹⁰ for reaction in the condensed phase.

The above diffraction experiments for CHT and CHD also reflect the nature of the nascent structures born at the point of descent to the ground state surface (the “transition state”). Both reactions have been the subject of recent *ab initio* calculations.^{6, 18} These calculations have suggested the existence of two regions on the excited-state energy surface, determined by the C–C stretch motion and the ring bending motion (a precursor to torsions). Also, the molecular structure at the conical intersection is highly distorted. If the conical intersection is reached directly in the initial motion, then femtosecond dynamics result, otherwise IVR is needed to redirect the trajectories. For example, at the point of descent from the excited state, CHT must adopt a near-planar geometry (as opposed to the minimum-energy boat-shaped geometry at equilibrium) for the [1,7]-sigmatropic hydrogen shift reaction to occur. Thus, efficient energy redistribution is essential in this transformation to the final geometry via a planar “transition state”. On the other hand, ring opening in CHD lands the structure in a highly asymmetric

geometry on the ground state and except for the subsequent hybrid (torsional and bond stretching) motion, the nature of the system is similar to that of the final product. In other words, the non-equilibrium features of the HT structure may reflect memory of an asymmetric geometry at the instant of ring-opening—suggesting that ring opening of CHD follows a symmetry-breaking pathway that violates the C_2 symmetry of the parent structure¹⁹. However, while *ab initio* calculations¹⁸ were performed for the minimum energy path, we are concerned here with nuclear dynamics of far-from-equilibrium structures. Thus, our diffraction results illustrate the crucial role played by structural changes in directing the subsequent dynamics in nuclear subspace (on the ground potential surface) of the reaction.

7.6 Review of Previous Studies in Light of Our UED Results

A. The Resonance Raman Studies of Mathies and co-workers^{20, 21}

Resonance Raman intensity analysis²⁰ has demonstrated that the initial excited-state evolution of CHD is along the conrotary reaction coordinate (as expected according to the Woodward–Hoffmann rules), and that depopulation of this state occurs in ~10 fs (determined from a linewidth analysis).

In 1993, Mathies and co-workers²¹ reported time-resolved UV resonance Raman studies of CHD→HT in the condensed phase. In their

results, the appearance time of the Stokes scattering from ground-state *cZc*-type HT is 6 ± 1 ps and the photoproduct anti-Stokes ethylenic intensity appears with a time constant of 8 ± 2 ps and decays in 9 ± 2 ps (this observation reflects the production and dissipation of “hot” HT-type product). Analysis of the photoproduct spectral evolution in the Stokes and anti-Stokes data as well as the observation of Raman lines characteristic of the *cZc* conformer in the anti-Stokes data demonstrates that *cZc* first appears on the ground-state surface, and then subsequently undergoes conformational relaxation to produce *cZt* with a time constant of about 7 ps. The photoproduct anti-Stokes ethylenic and single-bond stretch intensities further demonstrate that the initial photoproduct temperature at 4 ps is 1500 ± 500 K [a very reasonable observation when compared to the value we calculated for the expected “fully thermalized” temperature (~ 2100 K; they estimated ~ 1950 K for the initial product temperature) neglecting any dissipation of heat to the solvent] and that the cooling time is ~ 15 ps. It was also shown that the time scale for any final conversion of *cZt* to *tZt* takes longer than 200 ps.

We believe that these time scales and their interpretation do *not* contradict our UED results and interpretations. While the appearance time (6 ps) for the HT species is significantly shorter than what we measured (~ 30 ps), we believe that their faster rate can be at least *qualitatively* rationalized

by including the additional de-activation channel available in the condensed phase (i.e., the channeling of energy from CHD* into the bath via contact with the solvent, which efficiently quenches the reaction). If CHD* is quenched by the solvent with a time constant of about 7 ps, it would reduce the appearance time of HT from 30 ps to the 6 ps observed by Mathies *et al.*²¹ Alternatively, the solvent may alter the available phase-space in the excited state in some way, thus yielding a faster decay. However, since they were blind to the direct depletion of CHD*, it is difficult to say anything more definitive than that. Moreover, we note that the relaxing of HT product conformers takes considerable time, and requires the presence of the solvent; therefore, it is not surprising that we still see a highly non-thermal conformer distribution (with *cZc* dominating).

The Mathies results (inevitably) rely on *ab initio*-derived resonance-Raman spectra for the *cZc* and *cZt* conformers. For example, they state: “The presence of scattering at 829 cm⁻¹ [well into the ps regime] strongly argues for the presence of the all-*cis* conformer on the ground state surface.” This particular argument is based on the fact that neither the *ab initio cZt* or *tZt* spectra have frequencies anywhere near this region, whereas *cZc* is predicted via *ab initio* methods to have one at 849 cm⁻¹. Still, one might question the relevance of *ab initio* predictions of resonant Raman spectra (specifically, the *absence* of certain lines) for species at zero temperature involved in the

CHD→HT reaction, when it is known there is an *enormous* amount of energy bouncing around in HT. Indeed, it is this *potential* weakness that is invoked by Sension and co-workers to question the Mathies' interpretation²¹ that supports long-time (many ps) ring-opening.

B. The Initial Work of Sension and co-workers

Sension and co-workers²² used a complimentary technique of fs transient absorption spectroscopy to further investigate the rate of appearance of the *cZc* conformer from photoexcited CHD. One-color transient absorption signals of CHD in cyclohexane and methanol pumped at 262, 268, and 273 nm revealed a rising component of several ps. In their analysis, these authors made the following assumptions: 1) The *cZt* and *tZt* conformers, as well as the *cZc* conformer, are formed. 2) The quantum yield for the CHD→HT isomerization reaction was fixed at 0.4. 3) The oscillator strengths of the *cZc* and *cZt* conformers *were restricted* to be in the range of 0.25–0.5 and 0.5–1.0, respectively. 4) The oscillator strengths of the vibrationally hot *cZc* and *cZt* species *were restricted* to be *smaller* than those of the thermally equilibrated isomers. 5) The time constant of conformational relaxation from *cZc* to *cZt* *was constrained to 7 ps* as determined in the ps resonance Raman experiments of Mathies and co-workers described above.

Under the framework of their assumptions, the authors basically

concluded that the ring-opening reaction is finished essentially completely within 1 ps of excitation and suggested that the 6 ps appearance of resonance Raman scattering (of Mathies and co-workers) from the initial *cZc* photoproduct is somehow limited by vibrational relaxation in the ground state manifold. Sension and co-workers concluded that the assignment of a 6 ps time constant for the appearance of the *cZc* photoproduct (i.e., ring opening) was physically unreasonable, as it would require that the absorption cross section for the initially formed, vibrationally hot *cZc* be *two to three times higher* than the absorption cross section of the thermally equilibrated *cZt* photoproduct at all three probe wavelengths (at least within the other constraints of their model).

Neglected is the possibility that only *cZc* is formed in their solution without significant conversion into *cZt* or *tZt*. We also note that these authors were selective in using results from the Mathies work—they disregard the 6 ps ring opening assignment, yet actually use the 7 ps time constant assigned to *cZc*→*cZt* conformational relaxation in their model. Moreover, the transient absorption spectra for *cZc* and *cZt* are unknown. They admit that while calculations proved quantitatively unreliable, the calculations did successfully reproduce the trend of $\text{CHD} < cZc < cZt < tZt$. Their conclusions, however, are based on the application of somewhat complex models (with parameters that are not well-known, especially over the various conditions of

the experiment) to simple transient curves.

C. The Work of Fuss, Kompa, and co-workers

More recently Fuss and co-workers used the same technique of fs transient absorption¹³ to study the ring-opening dynamics of CHD and the subsequent processes such as isomerization and cooling in the condensed phase. The interpretations and time scales for the ring-opening and isomerization were drastically different from those of the Raman studies of Mathies and co-workers and were mostly consistent with the FTS studies of Sension and co-workers (which is not surprising, since the technique was the essentially the same). The interpretation starts from the analysis of the transient absorption at 404 nm of CHD dissolved in ethanol after excitation at 267 nm. Since CHD as well as HT absorb only at wavelengths shorter than 290 nm, this transient absorption at 404 nm was attributed to the excitation from the S_1 to higher electronic states S_n , requiring less energy than the excitation from the ground state to the S_1 state. The transient absorption signal clearly showed that the species giving the transient signal disappears within 300 fs. From this observation, they concluded that the ring-opening completes within 300 fs (i.e., $\text{CHD}^* \rightarrow \text{HT}$).

However, the observed behavior *might not be representative*, i.e., the conclusion is right (e.g., in this case, they are indeed seeing ring opening in

300 fs), but it is a picture only of what a small percentage of reacting molecules are doing, with the rest of the molecules being dark for some reason. Correspondingly, the second possibility is that the behavior is indeed representative of the entire ensemble, but the conclusion is wrong (e.g., in this case, the time constant *does not* represent ring opening, but merely results from the wave packet passing through a *narrow observation window* that happens to have a high absorption cross section at 404 nm compared with other species. Thus, the species giving a high absorption at 404 nm may not represent the *whole landscape* of the excited states (1B_2 and 2A_1) of CHD, and the ring has not opened yet, even after the wave packet passes through the 404 nm window).

The rest of the interpretation was merely based on this conclusion that CHD ring-opening occurs within 300 fs, and therefore, would be easily falsified if the initial conclusion were wrong. In their model, the concentrations of the conformers reach thermal equilibrium in a few picoseconds; during the first 10–20 ps, the concentrations follow the cooling of the molecule by the solvent, staying near thermal equilibrium (i.e., rapidly tending toward *tZt* in great majority); and a small quantity of *cZt*-hexatriene is trapped in its potential well on a time scale of 100 ps at the final temperature (300 K) (Note that *this* result is also very different from those of Mathies and co-workers). Their confidence about the short time scale for the

ring-opening process seems to have originated from their previous studies.²³ Also, see their later work in the gas phase¹⁵ where a short time scale was claimed. The earlier result of Sension and co-workers may have contributed to their biased assumption. Still, the authors spend a considerable amount of time deconstructing the results and interpretations of Mathies and co-workers, and make some strong arguments. While seemingly neglecting a few of Mathies' more qualitative yet convincing arguments (e.g., the presence/absence of particular resonances that could only be reasonably assigned to particular conformers), they directly challenge Mathies' quantitative interpretations. For example, they believe that if differences in transition dipole moments of the HT conformers were included by Mathies' group in their analysis, they would have concluded that their 6 ps rise was actually due to conformer isomerization, not ring opening. Additionally, Fuss and co-workers believe that one resonance assigned to *cZt* should have been assigned to *tZt*, leading Mathies to conclude that *tZt* was not appreciably formed over the course of their experiment, when in fact it was.

In their most recent study¹⁵ in the gas phase, the same researchers used dissociative intense-laser field ionization in an attempt to substantiate the ultrafast nature of the dynamics of CHD ring opening. All the transient mass signals showed very short time constants. On the basis of the rather different fragmentation pattern of CHD and HT when ionized by an intense-

laser field, the H^+ mass transient was attributed to the formation of HT. However, neglected is the possibility that the extremely strong laser fields may perturb the potential energy surfaces of the whole process of ring-opening and isomerization, instantly accelerating the ring-opening process and creating the product, thereby giving an artificially fast appearance time for the product.

However, we note that the potential problem with the intense-field ionization may be absent with the resonance-enhanced multiphoton ionization (REMPI) experiments performed by this group. Actually, the same authors²⁴ utilized time-resolved REMPI and obtained a 600 fs rise time, which was attributed to product formation by ring opening. However, later on they reassigned the 600 fs to the conformer isomerization in the hot product.

In other work by Sension and co-workers,²⁵ they expanded their transient absorption study in this system in solution. Their results and interpretations are almost identical to those of Fuss and co-workers.

7.7 Implications of UED Studies on Understanding IVR

The photo-initiated, non-dissociative radiationless decay processes in CHD embody a prototypical IVR problem. Indeed, there are two universal characteristics associated with this process that make this photo-reaction a particularly interesting case: (1) A vast amount of the electronic energy is

transferred to the vibrational energy of the molecule in a relative short period of time. (2) There is a direct coupling to the low-frequency skeletal torsion modes at higher vibrational levels. Because the reaction pathway connecting the ground and excited electronic levels is rather steep (with regard to the energy potential surfaces), and often begins with a well-characterized geometry, the initial condition of IVR (e.g., the geometry of the molecule and the locality of non-thermalized population distributions) is probably similar for all the molecules in the ensemble, albeit there is probably not a universal onset time for the decay of the molecules.

For CHD in particular, the ring opening is directly coupled to large-amplitude torsional motions along a potential well where the conformational barrier is rather low compared to the initial available vibrational energy. Here two questions come to mind: (1) In a collisionless environment, how is the energy which is initially deposited in the torsional modes (with their relatively high densities of state) coupled to other, higher-frequency modes of bond stretches and more rigid (higher-energy) torsional motions? (2) What is the time scale of this coupling, and how does it vary depending on the molecular environment and the nature of the excited-state preparation? In the gas phase, a very similar process is the collision-induced level-crossing non-adiabatic decay in bi-molecular reactions involving electronically excited species. Even more common in condensed phases is solvent-mediated non-

radiative decay, one of the primary energy channels in photolysis. Indeed, as indicated above, reaction dynamics may be greatly affected by the presence of solvent. Understanding the IVR process in the gas phase can also cast light on the effects of solvation in condensed phases. Additionally, while IVR is usually studied in the *energy domain* by following the frequency signatures associated with specific ro-vibrational motion of molecules, UED provides a different perspective in studying IVR by monitoring the structural evolution directly.

First, our result of a highly unexpected 1.7–1.8 Å C–C peak in the radial distribution curves suggests a rather long IVR time for the molecular motions coupled with this internuclear separation. This observation begs the question: what are the reaction coordinates involved in the manifestation of this extremely long bond distance? Perhaps a clue to the answer of this question lies in the conclusion that the averaged product structure is highly non-thermal, resembling an asymmetric *cZc*, or a more folded *cZt*, *even up to 400 ps after the reaction began*; thus, the non-thermal torsional motions around the C–C single bonds survive for at least 400 ps. As shown schematically at the top of Fig. 7–15, an inverted population in the torsional rotor mode has a higher probability to be seen in the geometries found near the classical turning points—i.e., the “folded” conformations found in both

halves of cZc (and one half of cZt)—in qualitative agreement with our observations.

As described elsewhere in this chapter, two attempts were made to theoretically explain the presence of the 1.75 Å peak. We reiterate that while the two fitting procedures used address the 1.75 Å peak in two rather different pictures, both models unmistakably assign the 1.75 Å peak to the C–C single bonds. In the first model, the origin of the averaged 1.75 Å peak is directly associated a non-Boltzmann population distribution of the local C–C stretching mode. A dual-Gaussian probability function was used to simulate a possible non-thermal bond-stretching. In such a scenario, the averaged 1.75 Å bond distance would originate from density at the *outer* classical turning point in the local Morse potential, whereas an averaged 1.4 Å distance would originate from density at the *inner* classical turning point. The energetics and eigenstate analysis showed that with 1.75 Å as the averaged outer turning position, the inner turning position should actually be around 1.2–1.3 Å, with a (demanding) mean vibrational energy of 25 kcal/mole *per bond*.

The second model, which employed a Monte Carlo search for the best-fitting Z -matrix representations of the averaged structure at each time point, instead indicated that one C–C bond was elongated to 1.75 Å while the other was somewhat shorter, at 1.35 Å (this is a subtle difference from the previous model, which considered *both* bonds to be in an *effective superposition* of long

and short). If one performs a calculation that adiabatically follows the *ab initio cZc* structure (with $\tau_1=\tau_2\sim 42^\circ$), stretching one of the C-C bonds to 1.75 Å takes about 10 kcal/mole. Also it is interesting to note that as the C-C bond was stretched, and the rest of the molecule was allowed to reorganize adiabatically from its initial *cZc* conformation, the molecule adopted a more open, asymmetric structure that is *not that different* from that obtained from the *Z*-matrix representation refinement of the effective averaged structure (e.g., with “G” referring to Gaussian, and “Z” referring to the *Z*-matrix data-refinement procedure, $\tau_1(\text{G})\sim 33^\circ$, $\tau_1(\text{Z})\sim 20^\circ$, $\tau_2(\text{G})\sim 59^\circ$, $\tau_2(\text{Z})\sim 63^\circ$) (Note that other structural features don’t compare as well—for example, Gaussian fails to make the second C-C bond shorter than the equilibrium value).

Thus, it could be argued that the second model—in which the long C-C distance really represents the time-averaged internuclear separation of one of the bonds, and which originates from coupling to the (manifestly non-thermal) torsional motion—provides a better, more self-consistent picture of the product structure and non-equilibrated behavior. Moreover, the preliminary analysis of the CHT data suggest that a *thermalized* model of hot CHT after internal conversion provides a good fit to the observed results (without requiring the existence a 1.75 Å C-C bond); this suggests that the non-thermal behavior manifested by the HT product results from the presence of the “floppy” torsional modes. This evidence provides further

support for the notion that the long CC single bond distance somehow originates from the non-thermal torsional mode vibrations.

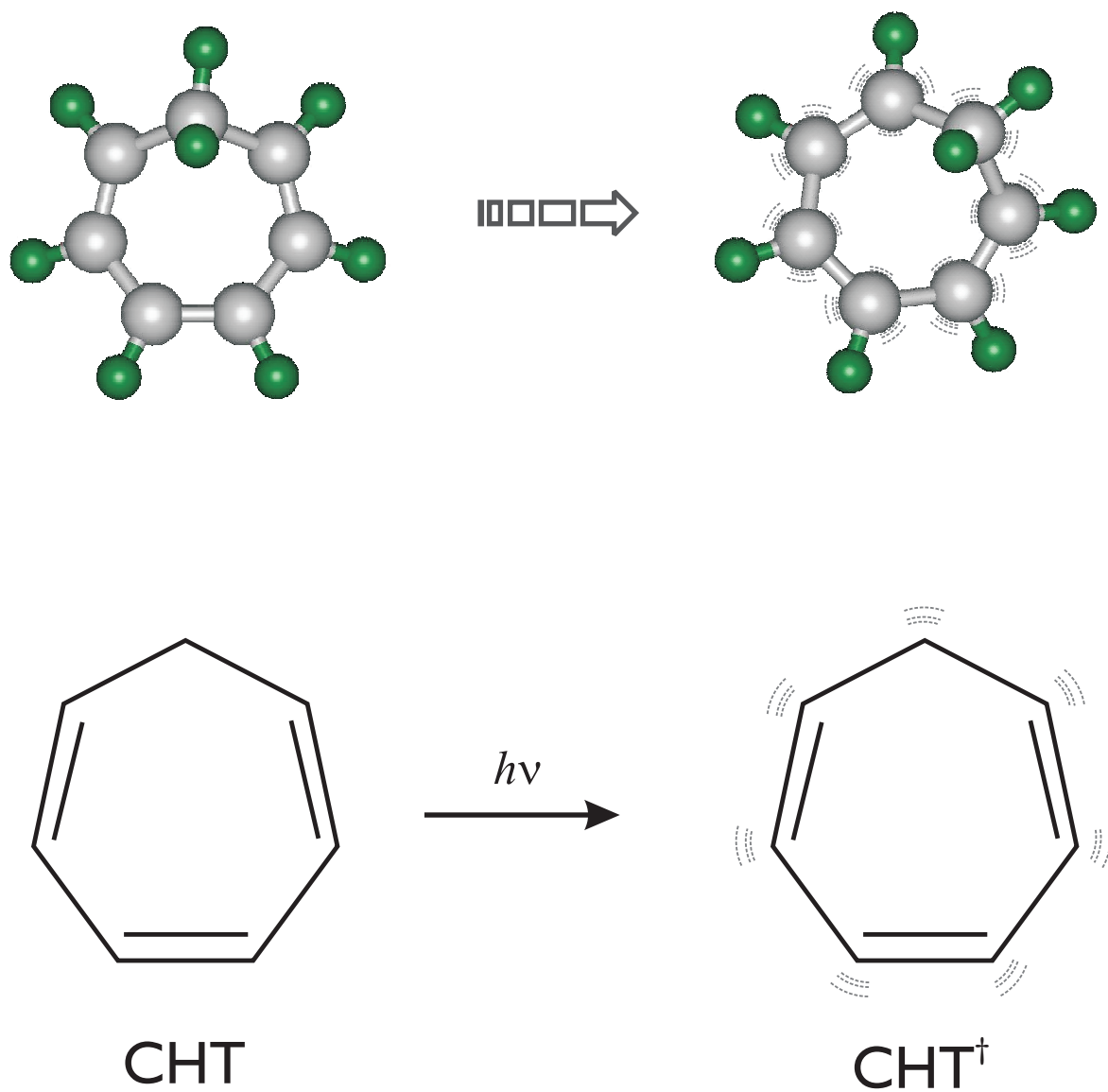
In a simple classical picture, one may visualize the two counter-propagating “rotors” of HT trying to pass by each other. At the classical turning points, the kinetic energy must be stored in the molecule, perhaps through stretching/compressing of the directly-coupled bond distances. In an *asymmetric* encounter, it is reasonable to stretch more on the faster moving arm as compared to the compression of the slow moving arm. This classical picture might be justified by the spatially localized initial preparation of a non-thermal ro-vibrational state resembling a wave-packet preparation on an excited vibrational manifold, and the close coupling of this motion to the reaction pathway following the ring-opening of CHD. (Note this classical “wavepacket” preparation refers to an *intramolecular* vibrational mode of a single molecule that just landed in the ground state surface. However, because the molecules leave the excited electronic surface randomly (characterized by a 33 ps life time), the preparation of the *ensemble* of molecules in the ground state surface is not a coherent one.) Additionally, it has been proposed that there is some long-lived “combination mode” comprised of the torsional motion and an asymmetric CC skeletal stretch, but we have not yet considered this possibility with any of our models.

Studies of vibrational motion with electron diffraction are complimentary to those performed with spectroscopic methods. The high-frequency local mode motions are associated with the mean amplitudes of vibration of the directly bonded distances. On the one hand, through the temperature effects seen via damping and frequency shifts in the molecular interference patterns caused by the increased mean amplitude motions, the local force fields can be extrapolated, complementing the spectroscopic information. On the other hand, the low-frequency large-amplitude motions can be studied through the changes of the indirect bond distances. The slow IVR processes associated with these motions, which usually are very hard to investigate directly by spectroscopic techniques, can now be studied by UED (as suggested in this work). The latter behavior is particularly relevant to larger, biologically-relevant systems. We should add that the analytical difficulties expected from such macromolecules are also addressed in our newly developed data-analysis procedures, in which the *Z*-matrix becomes the central pivoting element linking the molecular dynamical modeling of the UED data with the vastly available biomolecular structure databanks (not to mention freeing us from having to manually develop geometrically consistent equations for such macromolecules—no doubt a Herculean task). The separation of rigid-frame molecular motions from the floppy, often classical-

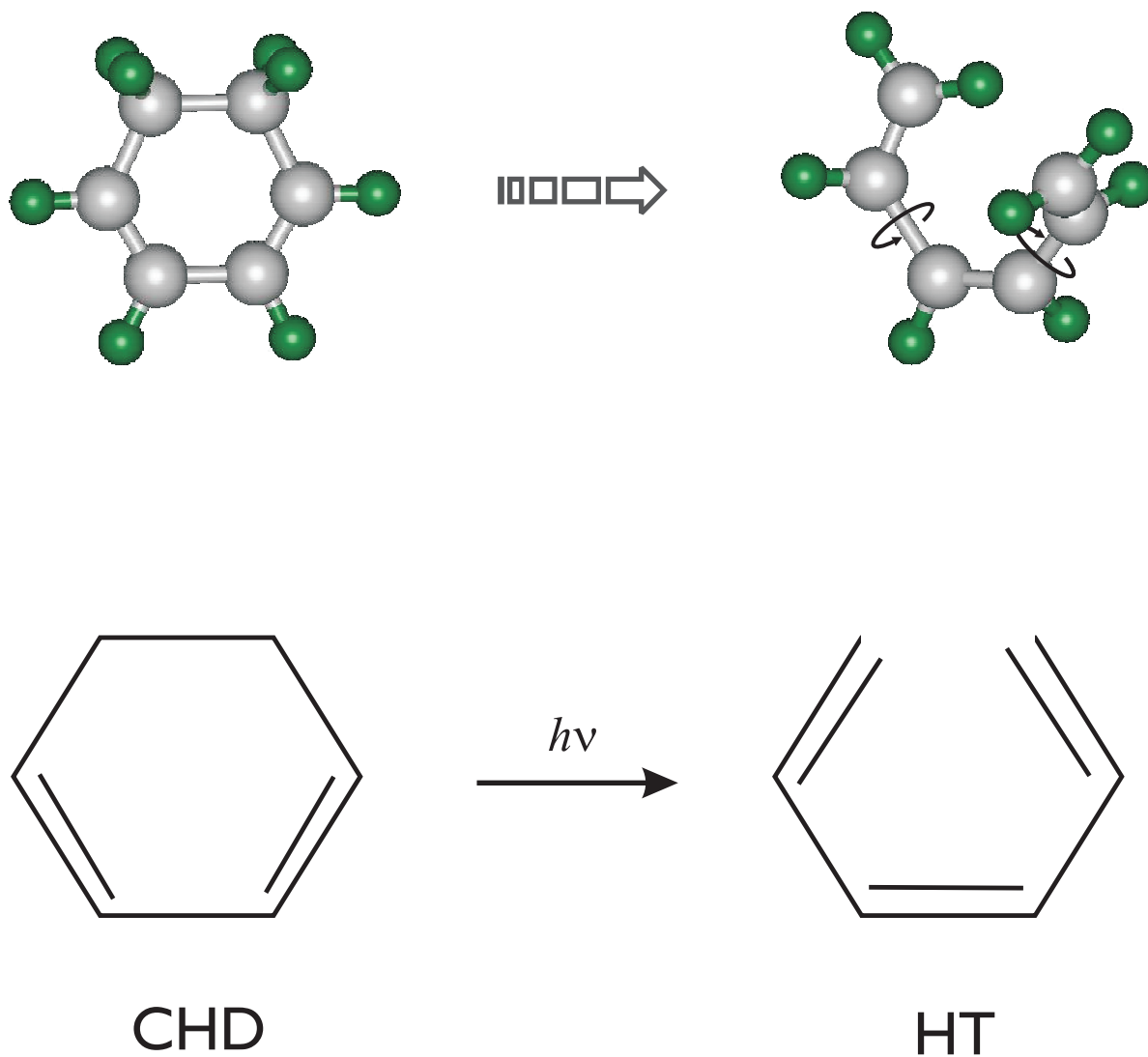
like, large-amplitude motions provides an additional advantage for using UED for studying complex molecular systems.

7.8 Conclusions

We have demonstrated the ability of ultrafast diffraction to observe the time evolution of molecular structures in non-equilibrium configurations. While non-thermal effects have been previously reported,²⁶⁻³¹ to our knowledge this is the first time that such far-from-equilibrium structures—in terms of both vibrational amplitudes and bond distances—have been directly observed in isolated complex molecules. The concept of negative temperature was invoked to describe the observed populations at high internal energies. The structural dynamics of the two hydrocarbons studied here underscore the importance of the following issues: (i) the critical influence of structural changes on energy redistribution and on persistence of certain bond motions; (ii) the nature of the nascent structure(s) born en route to the final product and the associated coherent dynamics; and (iii) the direct relevance of structural changes associated with bond breaking and making in understanding the disparities of measured time scales for state population dynamics in the condensed phase.



Scheme 7-1. Nonradiative decay of excited 1,3,5-cycloheptatriene (CHT) to 'vibrationally hot' ground state.



Scheme 7-2. Ring opening of 1,3-Cyclohexadiene (CHD) to form 1,3,5-Hexatriene (HT).

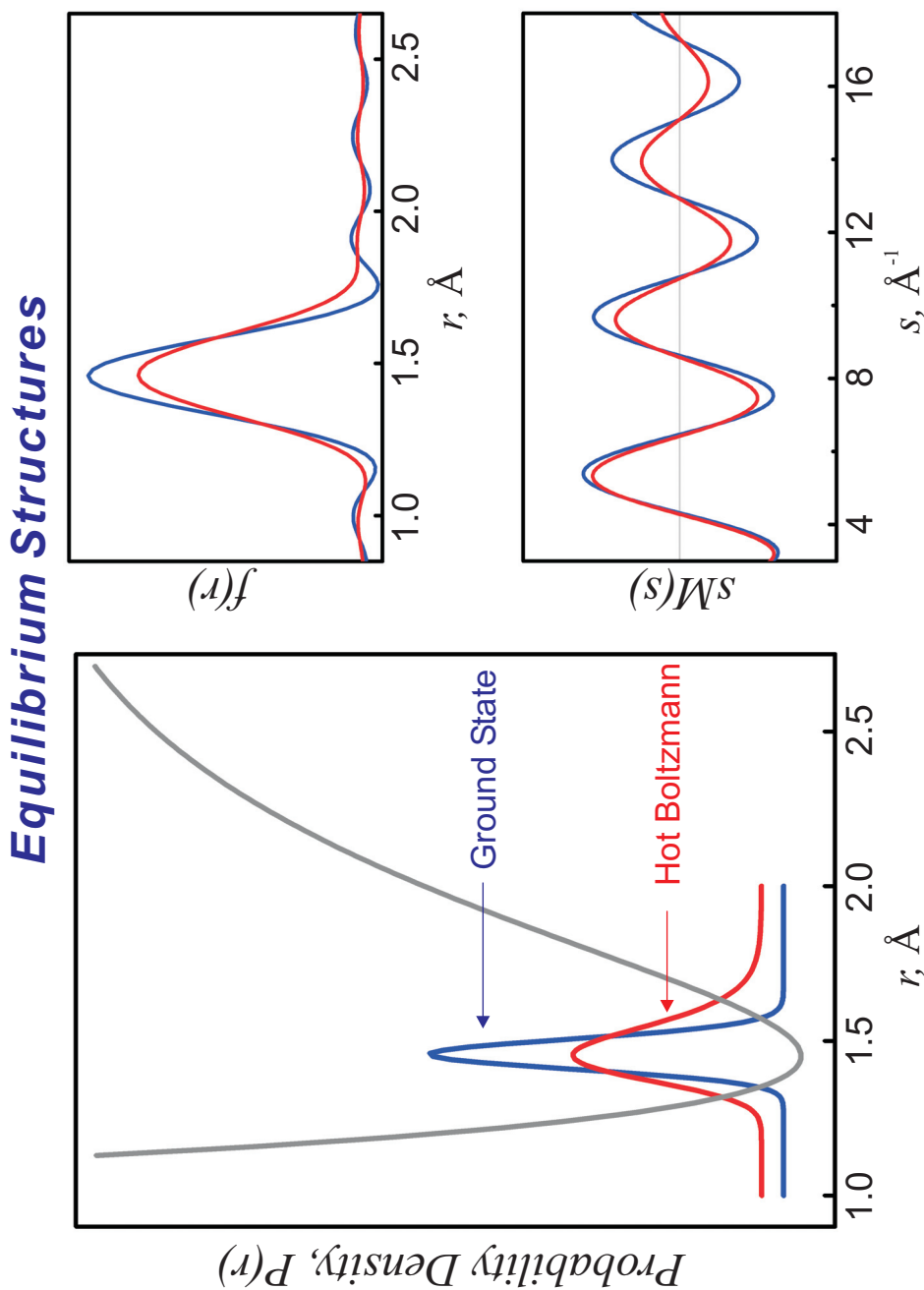


Figure 7-1. Calculated diffraction curves for a single bond in the *equilibrium* regime. Shown on the *left* are probability densities of the single bond distance, and on the *right* are the resulting $sM(s)$ and $f(r)$ curves. Thermal (Boltzmann) vibrational population at ground state is shown in blue and at a much higher temperature in red. Increased temperature results in broadening of the $f(r)$ curve and damping of the $sM(s)$ curve.

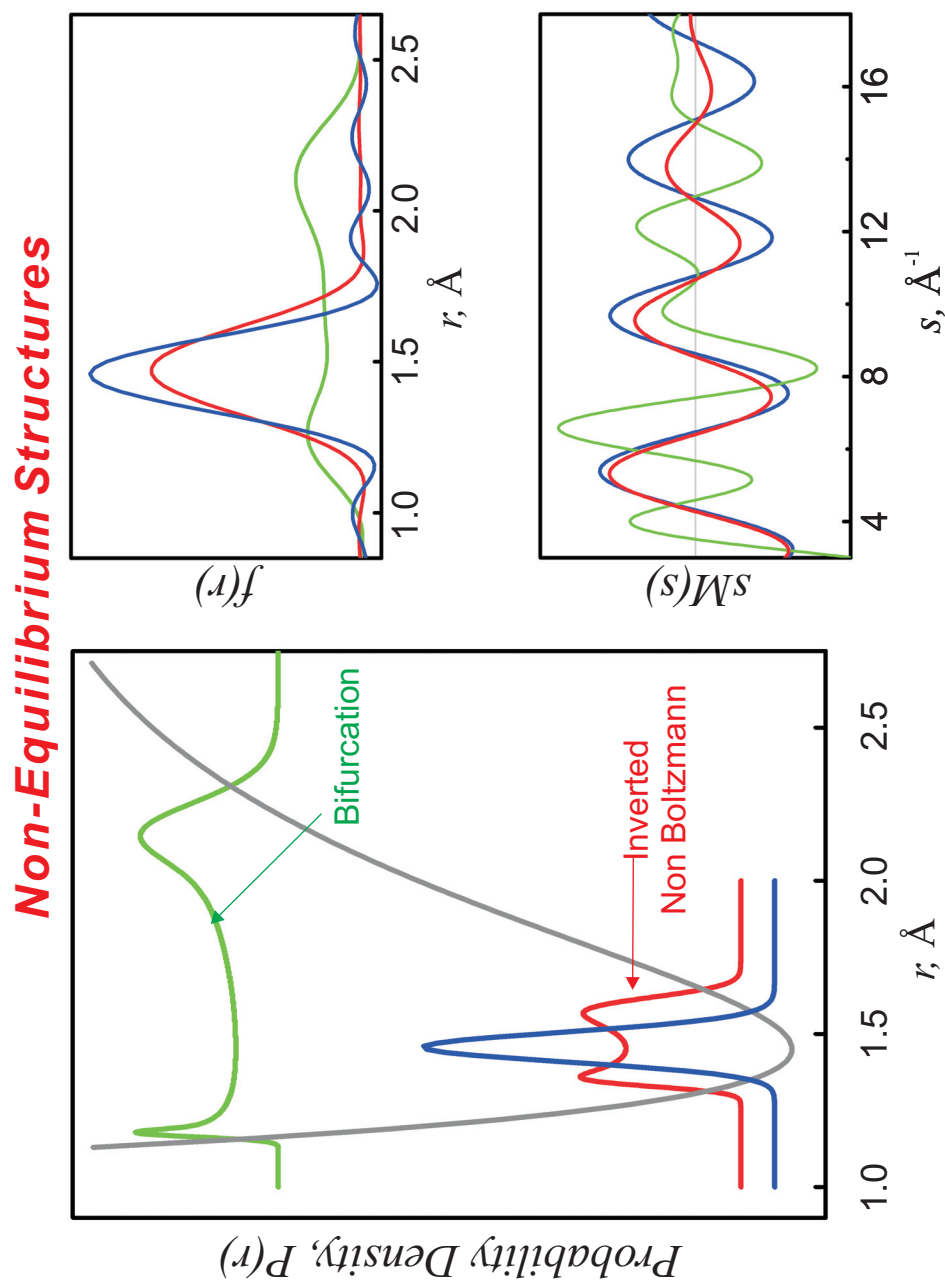


Figure 7-2. Calculated diffraction curves for a single bond in the *Non-equilibrium* regime. Shown on the *left* are probability densities of the single bond distance, and on the *right* are the resulting $sM(s)$ and $f(r)$ curves. Inverted (non-Boltzmann) vibrational populations are modeled with Gaussian distributions. Low-lying inverted populations (red) will cause broadening of the $f(r)$ curve and damping of the $sM(s)$ curve similar to the Boltzmann case above. Higher-lying populations (green) can lead to outright bifurcation of the internuclear density and significant changes in the frequency components of the $sM(s)$ scattering signal.

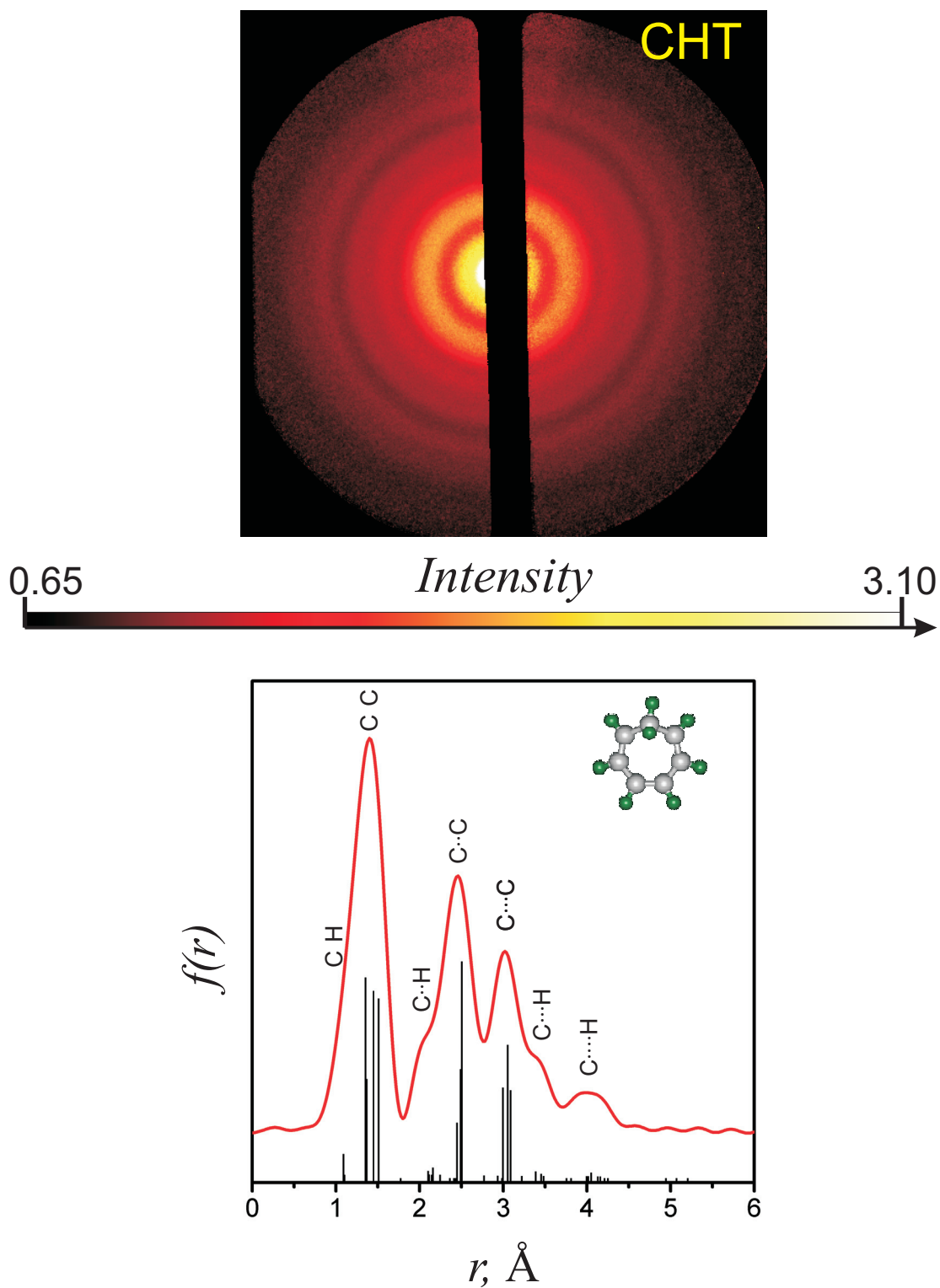


Figure 7-3. Observed ground-state diffraction image and corresponding $f(r)$ curve for CHT. The major bond distances (covalent C–C, second nearest-neighbor C·C, and third nearest-neighbor C··C) are shown above the corresponding $f(r)$ peaks.

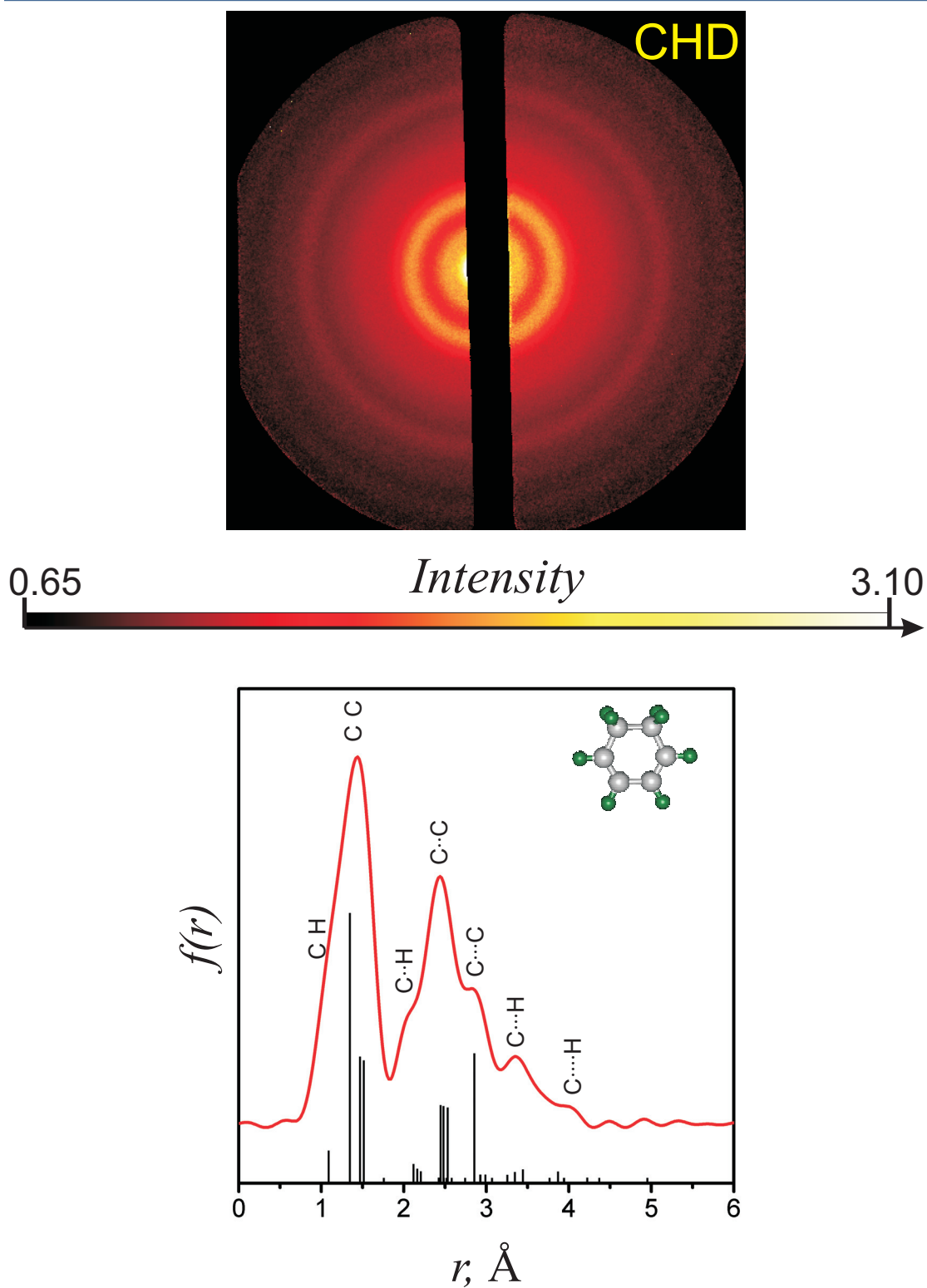
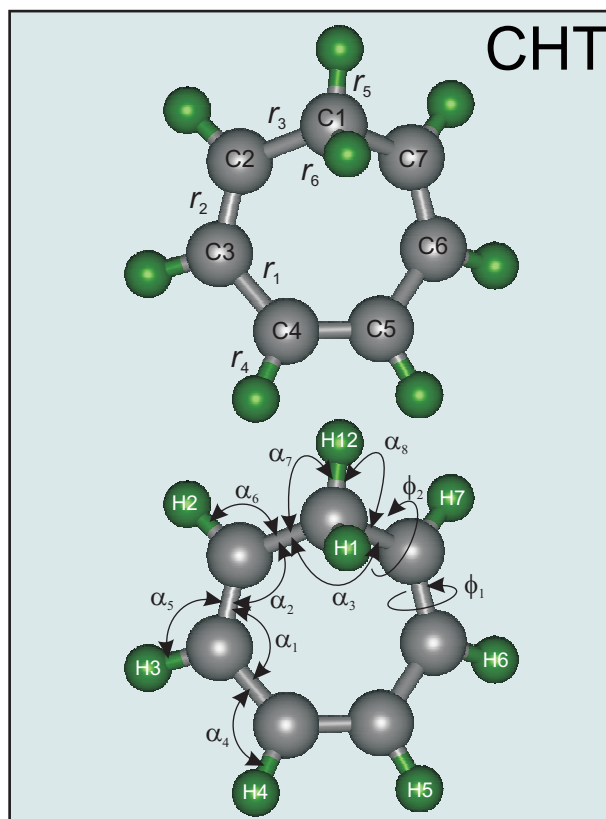


Figure 7-4. Observed ground-state diffraction image and corresponding $f(r)$ curve for CHD. The major bond distances (covalent C–C, second nearest-neighbor C·C, and third nearest-neighbor C··C) are shown above the corresponding $f(r)$ peaks.



Distances

$r_1(\text{C3-C4})$	$= 1.429 \pm 0.009$	(1.47)
$r_2(\text{C2-C3})$	$= 1.382 \pm 0.008$	(1.34)
$r_3(\text{C1-C2})$	$= 1.523 \pm 0.004$	(1.52)
$r_4(\text{C4-H4})$	$= 1.095 \pm 0.012$	(1.089)
$r_5(\text{C1-H12})$	$= 1.104 \pm 0.113$	(1.093)
$r_6(\text{C1-H1})$	$= 1.117 \pm 0.080$	(1.098)

Angles

$\alpha_1(\text{C2-C3-C4})$	$= 122.5 \pm 3.0$	(125.6)
$\alpha_2(\text{C1-C2-C3})$	$= 119.6 \pm 2.3$	(122.0)
$\alpha_3(\text{C2-C1-C7})$	$= 117.0 \pm 1.7$	(108.2)
$\alpha_4(\text{C3-C4-H4})$	$= 122.6 \pm 2.7$	(116.4)
$\alpha_5(\text{C2-C3-H3})$	$= 116.6 \pm 5.9$	(117.8)
$\alpha_6(\text{C1-C2-H2})$	$= 113.1 \pm 8.8$	(118.5)
$\alpha_7(\text{C2-C1-H12})$	$= 101.8 \pm 9.4$	(110.3)
$\alpha_8(\text{C7-C1-H12})$	$= 111.3 \pm 8.3$	(98.4)

Figure 7-5. Refined ground-state structure of CHT. The refined bond distances and angles are shown, along with the DFT values indicated in parentheses. Distances are in ångströms, and angles are in degrees.

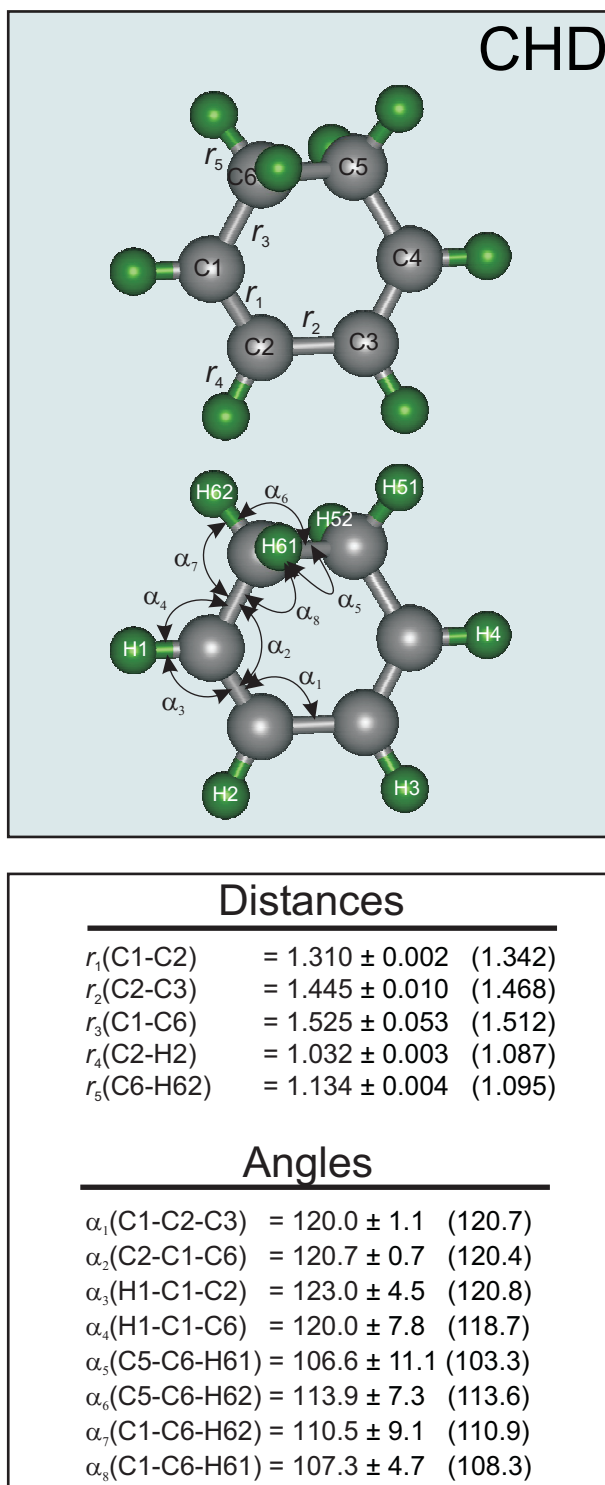


Figure 7-6. Refined ground-state structure of CHD. The refined bond distances and angles are shown, along with the DFT values indicated in parentheses. Distances are in ångströms, and angles are in degrees.

Non-Equilibrium CHT Structure

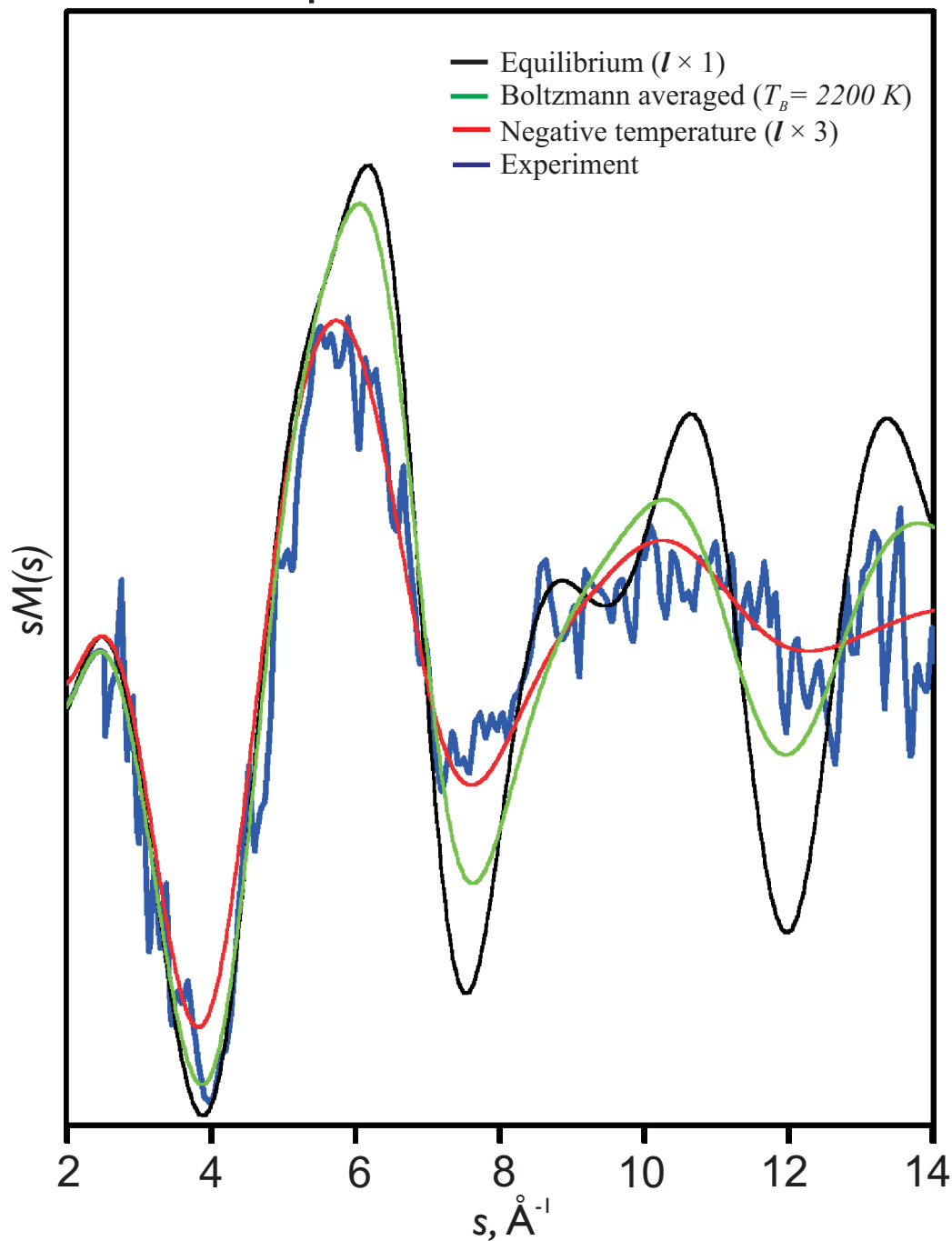


Figure 7-7. Non-equilibrium ‘negative temperature’ in CHT as reflected in the transient-only $sM(s)$ curves. The (blue) experimental curve averaged from 75 to 400 ps is shown, along with corresponding theoretical curves for the equilibrium structure at 403 K (black), the Boltzmann averaged structure at ca. 2,200 K (green), and a non-Boltzmann structure with a mean l value nearly three times that at 403 K (red). For details of structural analysis, see text.

Non-Equilibrium CHT Structure

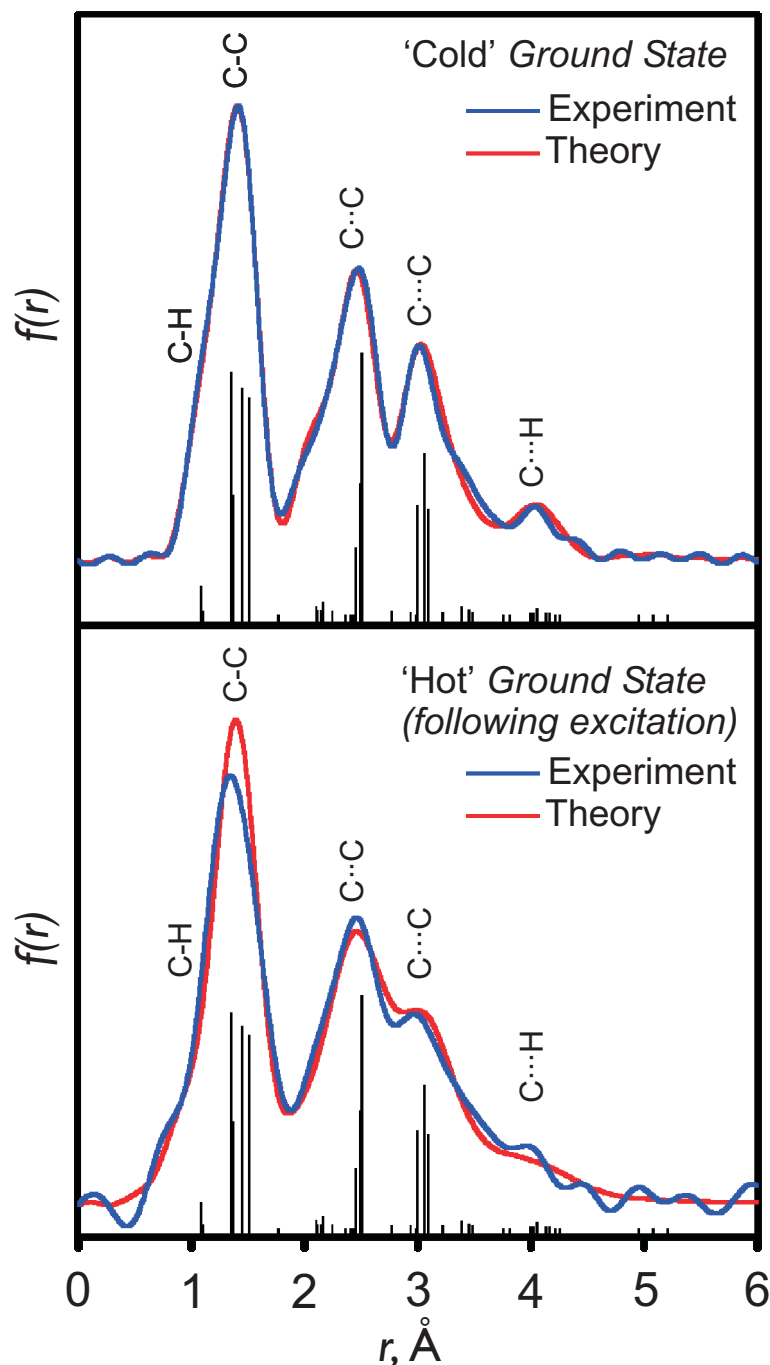


Figure 7-8. Non-equilibrium 'negative temperature' in CHT. Shown is the influence of high vibrational temperature on the ground-state and transient-only $f(r)$ curves. The $f(r)$ curves for the initial structure at 403 K (Top) and the hot CHT structure at a negative temperature (Bottom). Note the significant broadening of the $f(r)$ peaks in the hot structure compared to the cold ground-state; only l was adjusted.

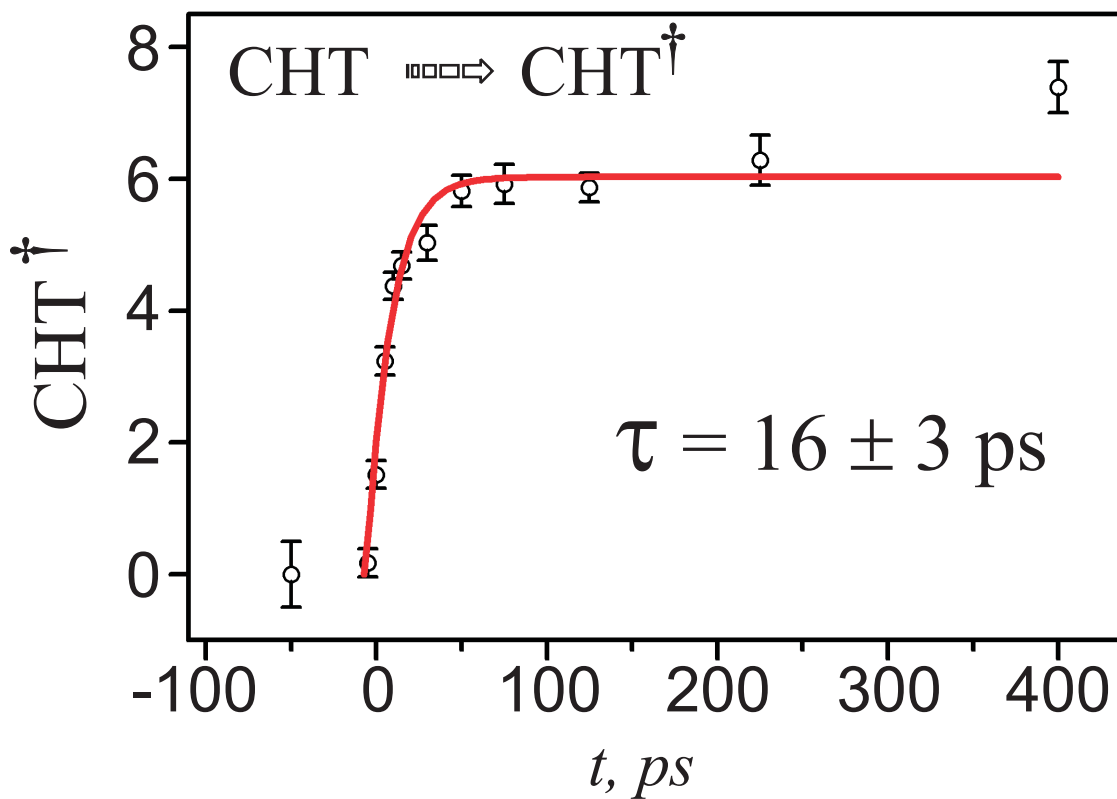


Figure 7-9. Evolution of transient non-equilibrium structure population in CHT.

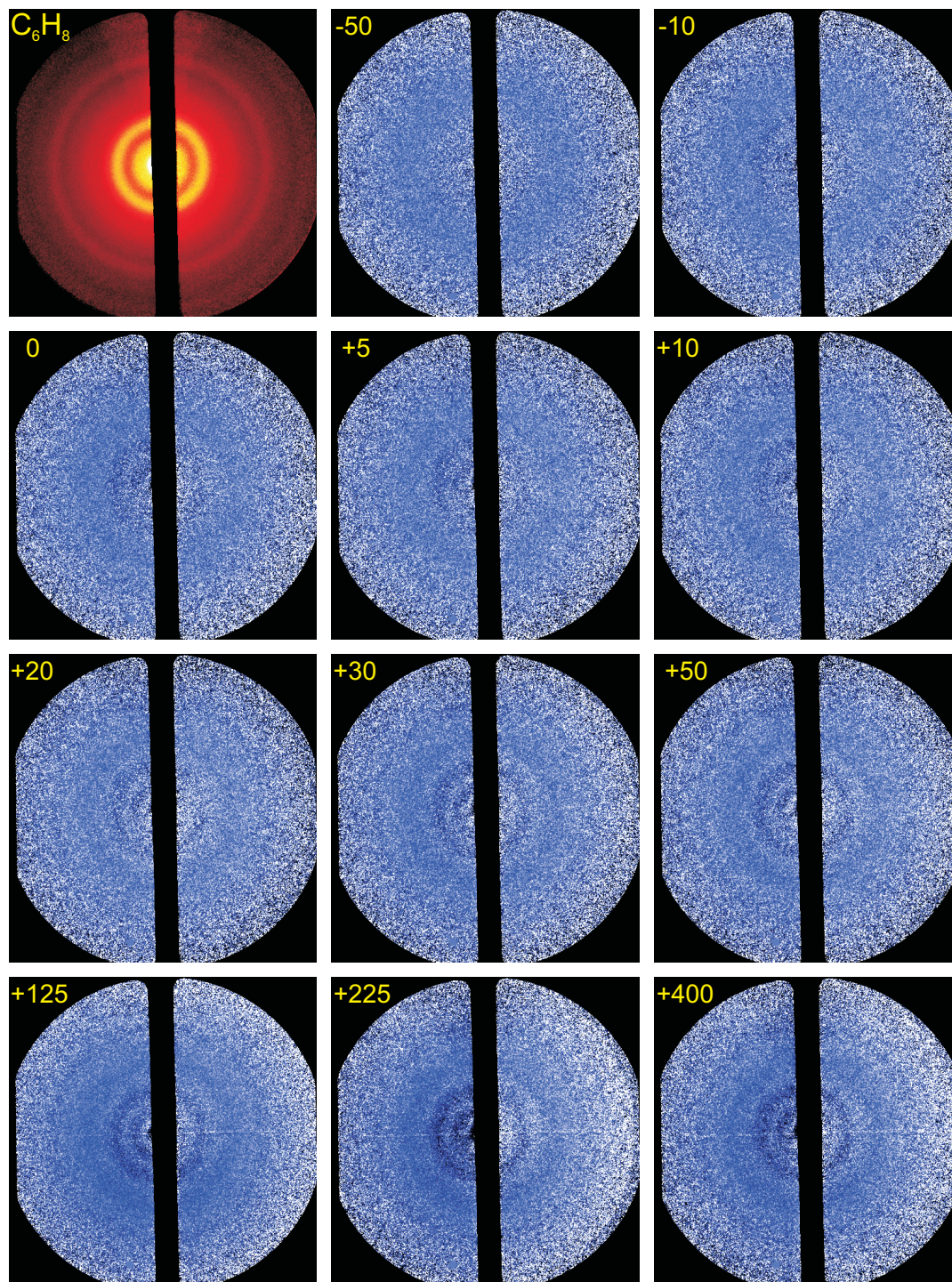


Figure 7-10. Time-resolved 2D diffraction-difference images of cyclohexadiene ($t_{\text{ref}} = -100$ ps). Each frame is identified by the relative time delay (in picoseconds) between the laser pump and electron probe pulses. The emergence of rings in the difference images with increasing time delay reflects the ensuing molecular structural dynamics. The first (*red*) image is the ground-state image.

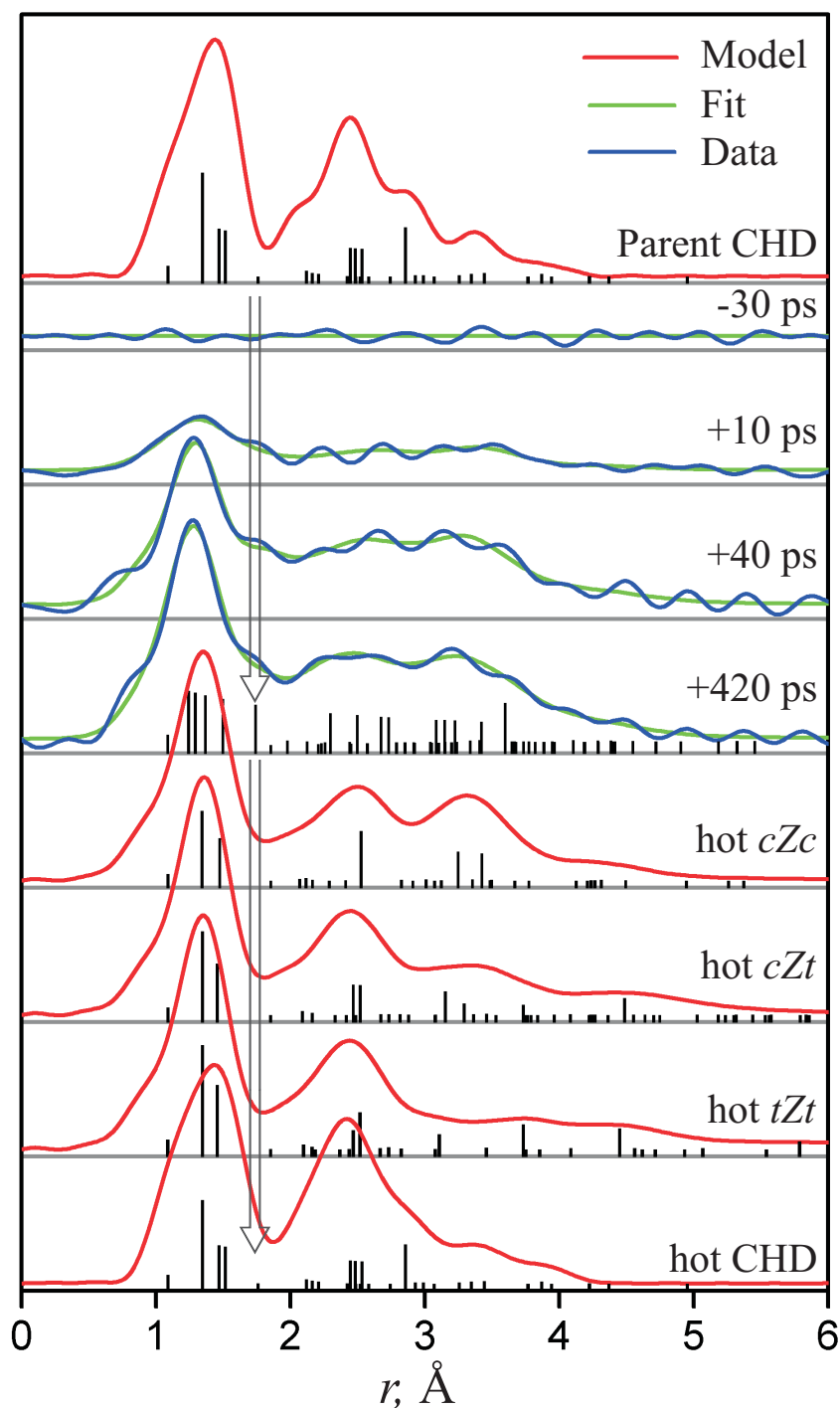


Figure 7-11. Time-resolved formation of hot HT structures after CHD ring opening. *Top:* DFT $f(r)$ curve (red) for the CHD parent structure at 403 K. *Middle:* comparison of selected experimental transient-only $f(t; r)$ curves (blue) with corresponding structural fits (green). *Bottom:* DFT $f(r)$ curves (red) for the three HT conformers (extrapolated to 2,100 K) and for hot CHD (extrapolated to 2,400 K) shown for comparison. The vertical arrows indicate the peak at ~ 1.7 Å, which is present in all experimental curves, but which is absent in the *ab initio* $f(r)$ curves of the three HT conformers.

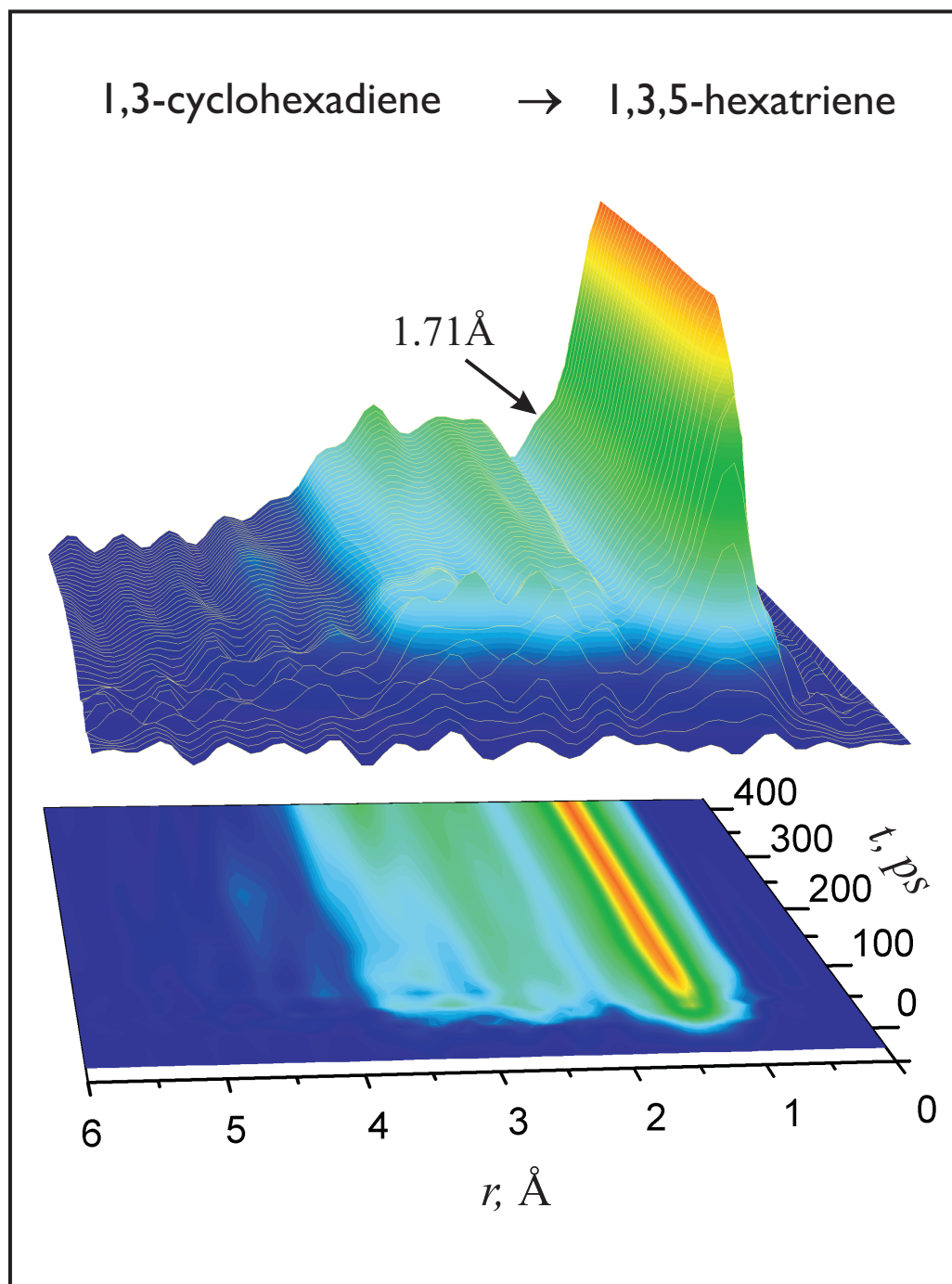


Figure 7-12. Time-resolved formation of hot HT structures after the ring opening of CHD. The Fourier-filtered $f(t; r)$ curves show product evolution over 400 ps; note the shoulder at $\sim 1.7 \text{ \AA}$.

Refined Ring-Opened Structure of HT

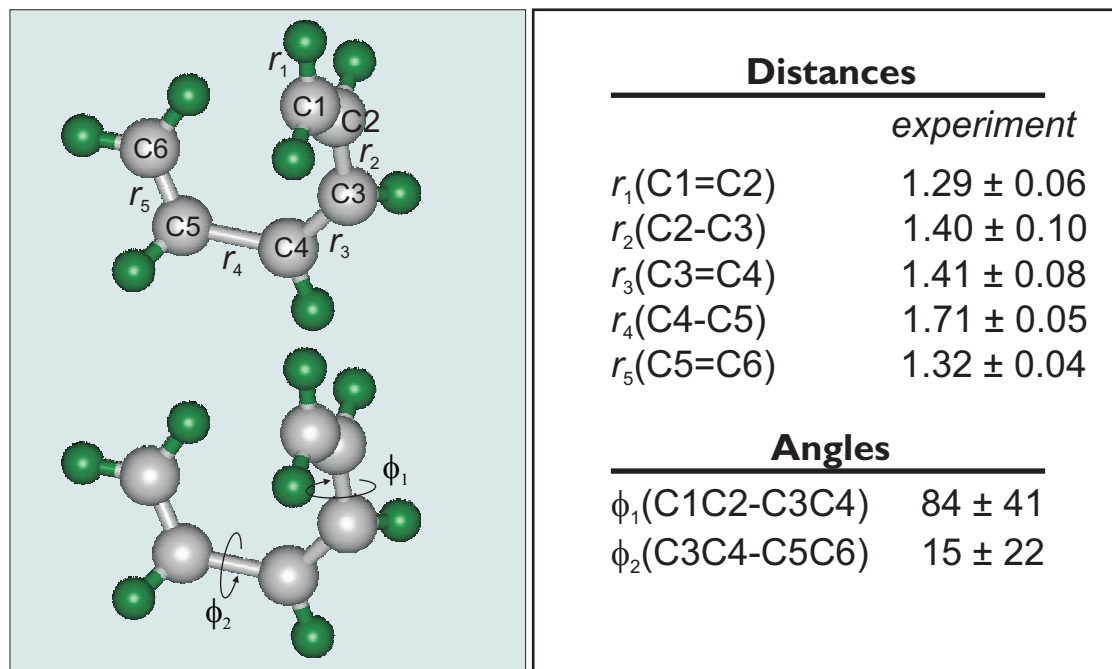
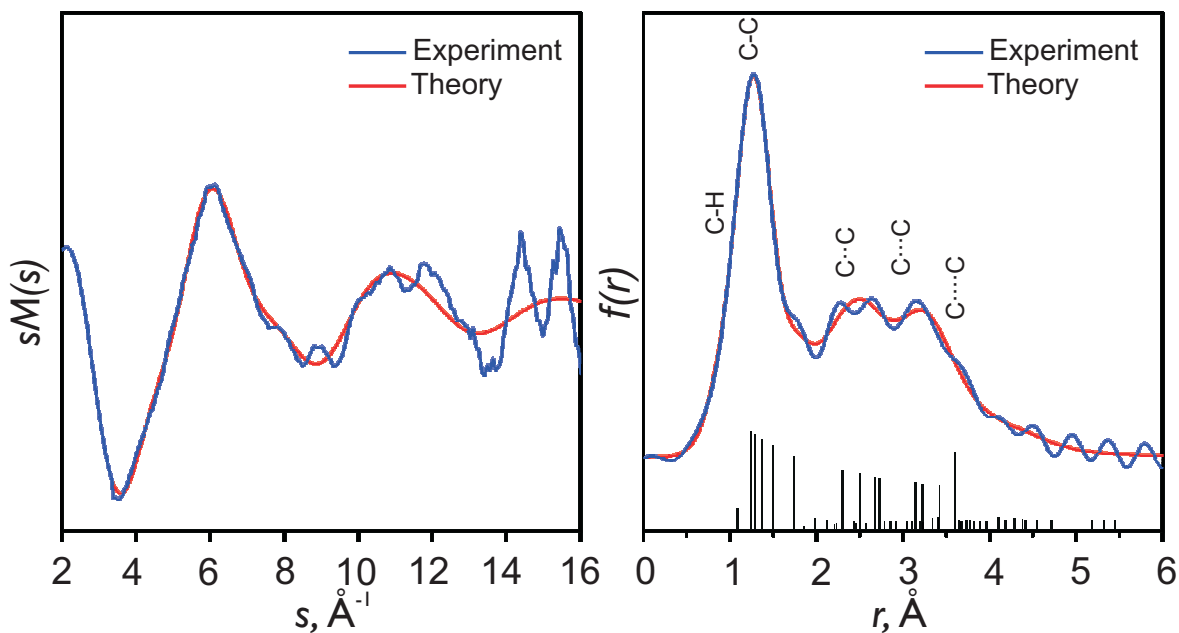


Figure 7-13. Structure refinement of ring-opened HT structure. Shown on *top* are the experimental $sM(s)$ and $f(r)$ curves, along with the best-fit theoretical curves. At the bottom is shown the refined HT structure, with its corresponding structural parameters. Distances are in ångströms, and angles are in degrees. The structural parameters were obtained by averaging over the Monte Carlo search results over all time points. The standard deviations represent the spread of the minimum basin in configuration space. Note the elongated (~ 1.7 Å) C4–C5 bond distance.

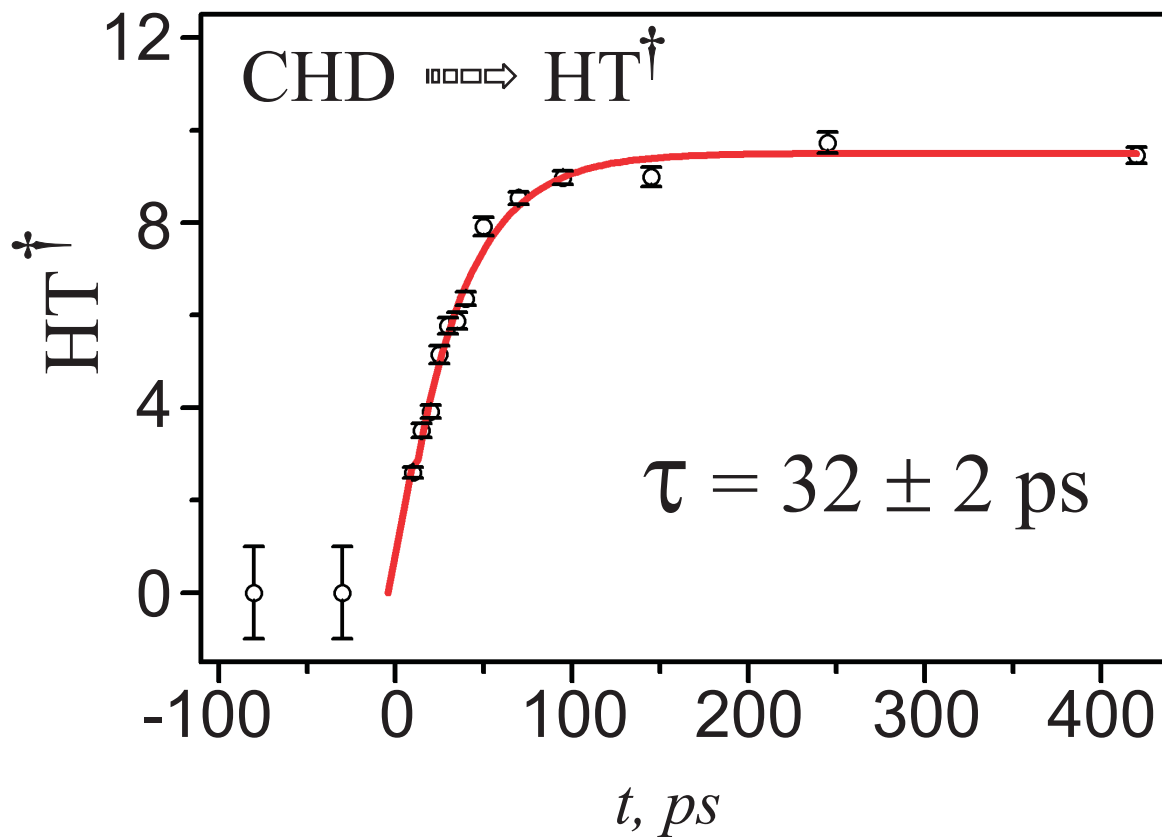


Figure 7-14. Evolution of transient *far-from-equilibrium* structure population in CHD. The time constant for the structural change in CHD is twice that in CHT.

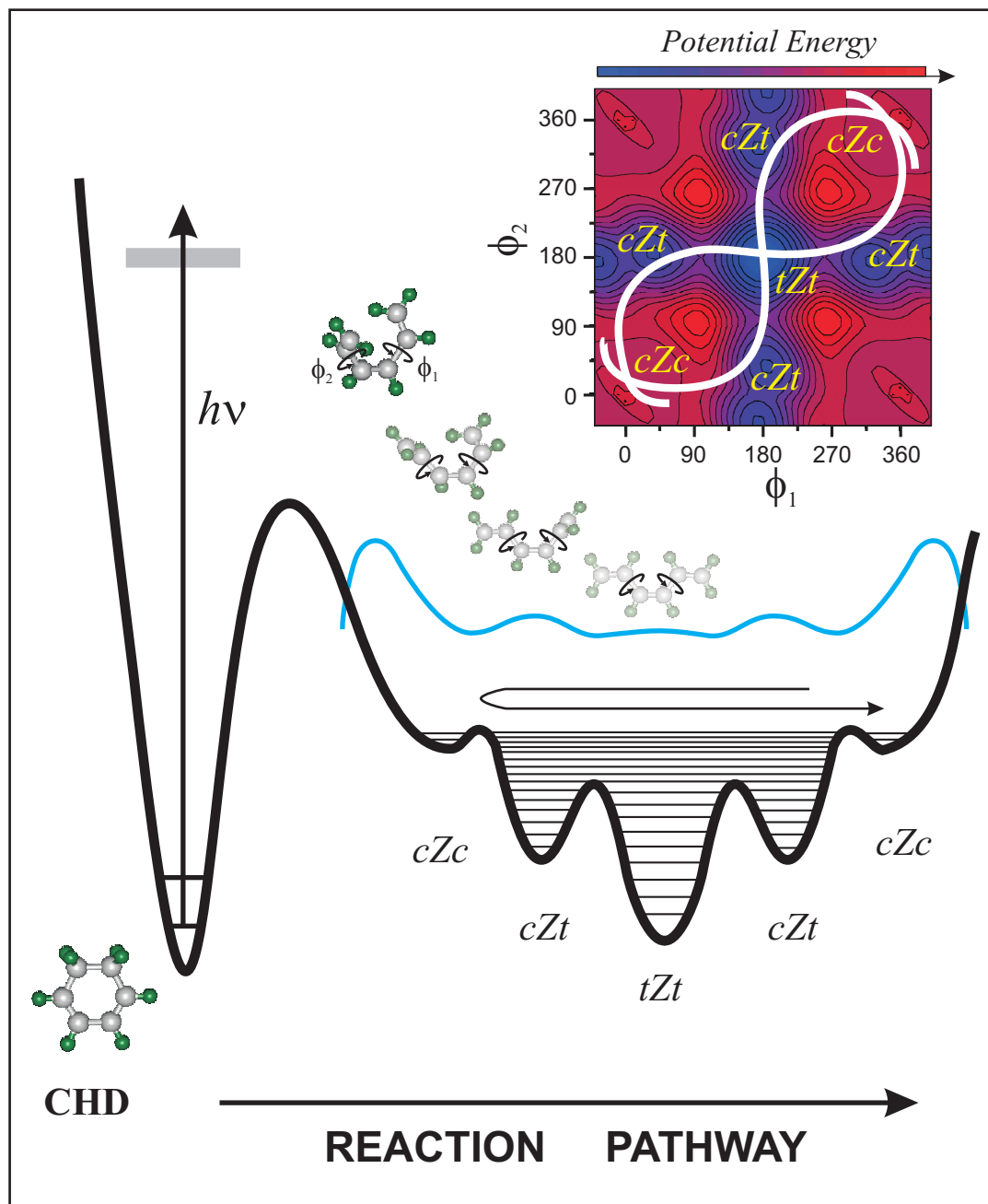


Figure 7-15. Potential energy landscape relevant to the formation of HT. A probability density curve (blue) on the schematic HT ground-state surface depicts the high-energy nature of the product structure. The higher density near the classical turning points reflects significant population in *cZc*-type conformations; the refined molecular structure shown at one of these points represents the average far-from-equilibrium structure over 400 ps. The “faded” structures denote the lower-energy *cZc*, *cZt*, and *tZt* conformations. Inset shows the corresponding *ab initio* 2D potential energy surface governing HT torsion angles (ϕ_1 and ϕ_2) about the C–C single bonds. The white curves illustrate possible trajectories leading to a time-averaged structure with considerable *cZc/cZt* character, but virtually no contribution from *tZt*.

Table 7-1. Selected refined structural parameters for the far-from-equilibrium HT structure

Structural Parameter	Mean [†]	s_{mean} [‡]	s_{fit} [§]	cZc	cZt	tZt
$r(\text{C1}=\text{C2})$	1.29 Å	0.06 Å	0.04 Å	1.338 Å	1.342 Å	1.342 Å
$(\text{C2}-\text{C3})$	1.40 Å	0.10 Å	0.02 Å	1.471 Å	1.453 Å	1.452 Å
$r(\text{C3}=\text{C4})$	1.41 Å	0.08 Å	0.04 Å	1.350 Å	1.353 Å	1.355 Å
$r(\text{C4}-\text{C5})$	1.71 Å	0.05 Å	0.02 Å	1.471 Å	1.465 Å	1.452 Å
$r(\text{C5}=\text{C6})$	1.32 Å	0.04 Å	0.03 Å	1.338 Å	1.341 Å	1.342 Å
$\phi_1(\text{C1C2}-\text{C3C4})$	84°	41°	11°	35.5°	-174.7°	180°
$\phi_2(\text{C3C4}-\text{C5C6})$	15°	22°	11°	35.5°	37.7°	180°

[†]Structural parameters obtained from averaging over all time points.

[‡]Standard deviation (spread) of the mean value.

[§]Standard deviation (error) of the least-squares fit.

^{||}Structural parameters for the HT conformers, calculated using *ab initio* methods (B3LYP/6-311G** basis set), shown for comparison.

References

1. Hargittai, I.; Hargittai, M., *Stereochemical Applications Of Gas-Phase Electron Diffraction*. VCH: New York, 1988.
2. Traetteberg, M., *J. Am. Chem. Soc.* **1964**, *86*, 4265.
3. Oberhammer, H.; Bauer, S. H., *J. Am. Chem. Soc.* **1969**, *91*, 10.
4. Reid, P. J.; Shreve, A. P.; Mathies, R. A., *J. Phys. Chem.* **1993**, *97*, 12691.
5. Trushin, S. A.; Diemer, S.; Fuss, W.; Kompa, K. L.; Schmid, W. E., *Phys. Chem. Chem. Phys.* **1999**, *1*, 1431.
6. Steuhl, H.-M.; Bornemann, C.; Klessinger, M., *Chem. Eur. J* **1999**, *5*, 2404.
7. Hertwig, A.; Hippler, H.; Schmid, H.; Unterreiner, A.-N., *Phys. Chem. Chem. Phys.* **1999**, *1*, 5129.
8. Paulick, W.; Jung, C.; Kempka, U.; Sühnel, J.; Gustav, K., *J. Mol. Struct.* **1981**, *85*, 235.
9. Möller, K. B.; Zewail, A. H., *Chem. Phys. Lett.* **1998**, *295*, 1.
10. Diau, E. W.-G.; Feyter, S. D.; Zewail, A. H., *J. Chem. Phys.* **1999**, *110*, 9785.
11. Yan, M.; Rothberg, L. J.; Callender, R., *J. Phys. Chem. B* **2001**, *105*, 856.
12. Lawless, M. K.; Wickham, S. D.; Mathies, R. A., *Acc. Chem. Res.* **1995**, *28*, 493.
13. Lochbrunner, S.; Fuss, W.; Schmid, W. E.; Kompa, K. L., *J. Phys. Chem. A* **1998**, *102*, 9334.

14. Andersen, N. A.; Pullen, S. H.; Walker II, L. A.; Shiang, J. J.; Sension, R. J., *J. Phys. Chem. A* **1998**, *102*, 10588.
15. Fuss, W.; Schmid, W. E.; Trushin, S. A., *J. Chem. Phys.* **2000**, *112*, 8347.
16. Clary, D. C.; Meijer, A. J. H. M., *J. Chem. Phys.* **2002**, *106*, 9829.
17. Minnard, N. G.; Havings, E., *Recl. Trav. Chim.* **1973**, *92*, 1315.
18. Garavelli, M.; Bernardi, F.; Olivucci, M.; Vreven, T.; Klein, S.; Celani, P.; Robb, M. A., *Faraday Discuss.* **1998**, *110*, 51.
19. Garavelli, M.; Bernardi, F.; Olivucci, M.; Vreven, T.; Klein, S.; Celani, P.; Robb, M. A., *Faraday Discuss.* **1998**, *110*, 51.
20. Trulson, M. O.; Dollinger, G. D.; Mathies, R. A., *J. Am. Chem. Soc.* **1987**, *109*, 586.
21. Reid, P. J.; Doig, S. J.; Wickham, S. D.; Mathies, R. A., *J. Am. Chem. Soc.* **1993**, *115*, 4754.
22. Pullen, S.; Walker, L. A.; Donovan, B.; Sension, R. J., *Chem. Phys. Lett.* **1995**, *242*, 415.
23. Trushin, S. A.; Fub, W.; Schikarski, T.; Schmid, W. E.; Kompa, K. L., *J. Chem. Phys.* **1997**, *106*, 9386.
24. Fuß, W.; Schikarski, T.; Schmid, W. E.; Trushin, S.; Kompa, K. L., *Chem. Phys. Lett.* **1996**, *262*, 675.
25. Pullen, S. H.; Anderson, N. A.; Walker, L. A.; Sension, R. J., *J. Chem. Phys.* **1998**, *108*, 556.

-
26. Zewail, A. H., *Angew. Chem. Int. Ed.* **2000**, *39*, 2587.
 27. Ischenko, A. A.; Schäfer, L.; Luo, J. Y.; Ewbank, J. D., *J. Phys. Chem.* **1994**, *98*, 8673.
 28. Mizutani, Y.; Uesugi, Y.; Kitagawa, T., *J. Chem. Phys.* **1999**, *111*, 8950.
 29. Helliwell, J. R.; Renzepis, P. M., *Time-Resolved Diffraction*. Oxford University Press: New York, 1997.
 30. Rouse, A.; Rischel, C.; Fourmaux, S.; Uschmann, I.; Sebban, S.; Grillon, G.; Balcou, P.; Forster, E.; Geindre, J. P.; Audebert, P.; Gauthier, J. C.; Hulin, D., *Nature* **2001**, *410*, 65.
 31. Techert, S.; Schotte, F.; Wulff, M., *Phys. Rev. Lett.* **2001**, *86*, 2030.